Petroleum Science 20 (2023) 3498–3515

Contents lists available at ScienceDirect

Petroleum Science

journal homepage: www.keaipublishing.com/en/journals/petroleum-science

Original Paper

Enhanced recovery of tight reservoirs after fracturing by natural gas huff-n-puff: Underlying mechanisms and influential factors

Chuan-Jin Yao [a, b, c, *], Ya-Qian Liu [a, b, c], Bai-Shuo Liu [a, b, c], Zheng-Dong Lei [d], Jia Zhao [a, b, c], Lei Li [a, b, c]

[a] National Key Laboratory of Deep Oil and Gas, China University of Petroleum (East China), Qingdao 266580, Shandong, China
[b] Key Laboratory of Unconventional Oil & Gas Development (China University of Petroleum (East China)), Ministry of Education, Qingdao, 266580, Shandong, China
[c] School of Petroleum Engineering, China University of Petroleum (East China), Qingdao, 266580, Shandong, China
[d] Research Institute of Petroleum Exploration & Development, PetroChina, Beijing, 100083, China

ARTICLE INFO

Article history:
Received 10 December 2022
Received in revised form
20 June 2023
Accepted 21 June 2023
Available online 28 June 2023

Edited by Yan-Hua Sun

Keywords:
Natural gas huff-n-puff
Matrix-fracture cores
Nuclear magnetic resonance (NMR)
Numerical simulation
Response surface method (RSM)

ABSTRACT

Tight oil resources are abundant in the world. It is very important to strengthen the research on the development theory and technology of tight oil reservoirs for ensuring national energy security. Natural gas huff-n-puff can effectively improve the oil recovery of tight oil reservoirs. However, the pore-scale oil production characteristics and the mechanisms of natural gas huff-n-puff in matrix-fracture cores are poorly understood. The influence degree of important factors on oil recovery is not clear and the interactions between factors are rarely considered. In this paper, the oil production characteristics and mechanisms of natural gas huff-n-puff in tight cores with different fracture lengths were quantitatively analyzed by combining nuclear magnetic resonance (NMR) with numerical simulation technology. The influencing factors and their interactions were evaluated by the response surface method (RSM). The results show that tight cores mainly consist of medium pores (0.1–1 μm) and small pores (0.01–0.1 μm). The fracture mainly increases the proportion of macro-pores (1–10 μm) and medium pores. In the natural gas huff-n-puff process, crude oil from macro-pores (1–10 μm) and medium pores is mainly developed, and the contribution percentage of crude oil in medium pores to oil recovery is the largest, up to 98.28%. The position of gas–oil contact (GOC) moves deeper as the number of huff-n-puff cycles increases. The contents of CH_4 and CO_2 in the oil phase remain at a high level within the GOC, while between the GOC and the component sweep front, the contents of CH_4 and CO_2 in the oil phase decrease with the increase in dimensionless distance. The gas component sweep volume is increasing with the increase in fracture length. Moreover, the injected natural gas mainly extracts C_3–C_{10} components from crude oil. The reduction law of crude oil viscosity is consistent with the migration laws of CH_4 components along the path. Compared with soaking time and gas diffusion coefficient, the injection pressure is the most significant factor underlying the recovery of natural gas huff-n-puff in tight cores. Besides the influence of single-factor, the interaction effects of gas injection pressure and diffusion also should be considered to determine the huff-n-puff parameters in the field implementation of natural gas huff-n-puff in tight reservoirs after fracturing.

© 2023 The Authors. Publishing services by Elsevier B.V. on behalf of KeAi Communications Co. Ltd. This is an open access article under the CC BY-NC-ND license (http://creativecommons.org/licenses/by-nc-nd/4.0/).

1. Introduction

With the rapid depletion of conventional resources, the petroleum industry has shifted more attention to unconventional resources, especially tight oil and gas, which have rich reserves and huge development potential (Yang et al., 2015; Syed et al., 2022). A large number of laboratory experiments, numerical simulations, and field tests have proved that CO_2 can effectively improve tight oil recovery (Song and Yang, 2013; Gamadi et al., 2014; Wang et al., 2017). However, the CO_2 injection technique is limited by gas sources. It is easy to cause asphaltene precipitation, resulting in

* Corresponding author. National Key Laboratory of Deep Oil and Gas, China University of Petroleum (East China), Qingdao 266580, Shandong, China
E-mail address: cy375@upc.edu.cn (C.-J. Yao).

https://doi.org/10.1016/j.petsci.2023.06.008
1995-8226/© 2023 The Authors. Publishing services by Elsevier B.V. on behalf of KeAi Communications Co. Ltd. This is an open access article under the CC BY-NC-ND license (http://creativecommons.org/licenses/by-nc-nd/4.0/).

blocking the seepage channels of tight reservoirs. Compared with CO_2, CH_4 is less corrosive, with a much lower increment in asphaltene precipitation than CO_2 (Shen and Sheng, 2016; Zanganeh et al., 2018; Zheng et al., 2021). Moreover, CH_4 and CO_2 have similar effects on the physical properties of crude oil, resulting in similar mechanisms of gas injection development, such as swelling crude oil and reducing oil viscosity. The miscible ability is stronger when natural gas contains more C_2 and C_3 components. It facilitates the production of remaining oil that is difficult to flow due to the capillary pressure (Hawthorne et al., 2016; Yu et al., 2020). Ozowe et al. (2020) compared the huff-n-puff effects of single-component N_2, CO_2, C_1, C_2, and different combinations of C_1, C_2, and C_3 by using numerical simulation technology. They found that gas with more C_1 exhibited higher oil production rates at the early stage of huff-n-puff, while gas with higher C_2 and C_3 contents gained higher oil recovery at the later stage of huff-n-puff. Alharthy et al. (2018) demonstrated that the hydrocarbon recovery for the Middle Bakken core during the solvent mixture of C_1 (85%) and C_2 (15%) soaking was up to 95% in 24 h. More importantly, associated gas is more readily available gas in the fields. Moreover, gas flooding can lead to fingering and gas channeling between connected wells in tight reservoirs, making the volume of injection gas swept small (Sanchez-Rivera et al., 2015). Huff-n-puff is the more suitable technique for the development of tight reservoirs. Field tests have demonstrated that gas huff-n-puff can significantly increase crude oil production (Hoffman, 2018; Orozco et al., 2020). Therefore, natural gas huff-n-puff in tight reservoirs was investigated in this paper.

Natural gas huff-n-puff can effectively improve tight oil recovery. However, the current experimental and numerical simulation studies mainly focus on the analysis of production effects. The pore-scale mechanism of natural gas huff-n-puff is rarely investigated. In particular, the oil production and remaining oil distribution of different pore spaces are very important for analyzing the microscopic mechanism. Fortunately, NMR technology can effectively characterize the distribution of fluid in porous media (Yang et al., 2013; Ma et al., 2019; Li et al., 2020a; Zhang et al., 2021). Wang et al. (2018a) achieved a quantitative analysis of oil recovery at the pore scale for the tight matrix exposed to CO_2 by the NMR T_2 spectrum. Wei et al. (2019) conducted experiments on CO_2 and N_2 flooding in the tight cores from the Lucaogou Formation, monitored the production dynamics using low-field NMR, and analyzed the pore-scale oil production mechanism. Song et al. (2022a) used NMR technology to measure residual oil distribution and oil production capacity in different pores to compare the potential of N_2 and CO_2 huff-n-puff to enhance tight oil recovery.

The oil-recovery mechanisms involved in a gas huff-n-puff process mainly include oil swelling, oil-viscosity reduction, mass transfer in two-phase, and reducing interfacial tension by achieving miscibility (Carlsen et al., 2019; Burrows et al., 2020). For rich gases, oil swelling and viscosity reduction dominated huff-n-puff recovery, while for lean gas, vaporization is the main huff-n-puff recovery mechanism (Alzobaidi et al., 2022). Min et al. (2020) obtained the same conclusion that the vaporization effects could contribute to the high recovery. Tran et al. (2020) introduced a ratio of convective to diffusive forces to quantitatively evaluate gas-transport and oil-recovery mechanisms. The results show that molecular diffusion is the dominant mechanism as the soaking period progressed. Gas expansion is the dominant oil-recovery mechanism, followed by system compressibility, oil swelling, and vaporization. The interfacial interactions between crude oil and gas including gas solubility, oil swelling, the oil diffusion coefficient, and interfacial tension, were also investigated (Li et al., 2020b; Tran et al., 2020). Therefore, this work chose the following parameters to evaluate the huff-n-puff performance, including the position of GOC, the mass transfer between oil and gas phases (including oil vaporization and gas solubility), and the oil viscosity reduction. However, the natural gas huff-n-puff mechanisms and performances in matrix-fracture cores are poorly understood. In particular, volumetric fracturing is an economic and effective measure to enhance tight oil recovery due to the extremely low matrix permeability of tight reservoirs (Du et al., 2014; Li et al., 2015; Sheng, 2017). Hence, this work makes three tight cores with different fracture lengths, and then the natural gas huff-n-puff mechanisms in matrix-fracture cores are studied.

In addition, the effects of the main factors on the natural gas huff-n-puff performance are equally essential. Li and Sheng (2017) analyzed the impact of diffusion, soaking time, and operation schedule on oil recovery based on the calibrated simulation models. The influence of natural fracture spacing, gas injection pressure, huff-n-puff cycles, and gas diffusion rate on CO_2 penetration depth was also studied using the field-scale simulation models (Li et al., 2018). The effects of gas injection pressure, soaking time, and fracture on the oil recovery during CO_2 huff-n-puff process were also investigated (Song and Yang, 2017; Huang et al., 2022). In the huff-n-puff process, the injected gas contacts the crude oil to transfer mass and achieve miscibility. The gas miscible production significantly enhanced the tight oil recovery. The soaking time affects the diffusion distance of injected gas. The injection pressure affects the degree of natural gas miscibility. The diffusion of injected gas in the oil phase affects the mass transfer in two-phase and gas penetration depth. However, many existing studies only conducted single-factor analysis, which did not fully consider the interaction between factors. It is difficult to determine the influence degree of each factor. RSM is a method to determine the correlations between multiple explanatory variables and response variables, which can be used to evaluate the influence degree of various factors and their interactions (Zuloaga et al., 2017; Afari et al., 2022; Wang et al., 2022). Therefore, RSM was used to perform sensitivity studies with three factors, including injection pressure, soaking time, and diffusion coefficient in this work.

In this paper, based on non-fracture, half-fracture, and penetrating-fracture cores, laboratory experiments and core-scale numerical simulations of natural gas huff-n-puff were conducted. The pore-scale oil production mechanism of natural gas huff-n-puff was quantitatively analyzed using NMR technology. Based on the numerical simulation models matching the experiments, the position of GOC, the characteristics of mass transfer between oil and gas phases, and the reduction law of oil viscosity were quantitatively analyzed. The single-factor analysis was conducted on the three influencing factors of gas injection pressure, soaking time, and diffusion coefficient. The sensitivity analysis was carried out using RSM. The research presented in this paper is of great significance to comprehensively understand the mechanism of natural gas huff-n-puff in matrix-fracture cores and clarify the influence law of the factors to improve tight oil recovery.

2. Huff-n-puff experiments

2.1. Materials

The experimental core samples were collected from the X block of Changqing Oilfield in the Ordos Basin. The porosity of these core samples ranges from 7.0% to 10.7%, and the permeability is from 0.01 to 0.46 mD. Three cores with similar permeability and porosity were selected to make non-fracture core, half-fracture core, and penetrating-fracture core. The purpose is to reduce the difference in basic core properties for studying the effect of the fracture length on natural gas huff-n-puff. The core samples were cut along the longitudinal direction from the end face by using the core cutting

device. The half-fracture core was created by cutting both ends of the core by 1/4 length. The penetrating-fracture core was made by cutting the entire core length. Then the fractures were evenly filled with the mixture of quartz sand and glue (Wang et al., 2020; Xia et al., 2022). The glue used was a mixture of epoxy resin adhesive and epoxy curing agent. And the volume ratio of quartz sand to glue was 10:1. Lastly, the cores were put in the oven to dry for 6 h. The fracture width is 1.4 mm and the permeability is 68.02 mD. The permeability of artificial cores which were made with the same volume ratio of quartz sand to glue was measured and the fracture permeability was determined by multiple measurements. The specific properties of the three cores are listed in Table 1, where core permeability refers to the permeability of the core samples before being cut. Fig. 1 shows the schematic diagram of three cores with different fracture lengths, where the length sum of the left and right fractures in the half-fracture core is 65 mm.

The experimental oil used in this work was from the Changqing Oilfield. The viscosity and the bubble point pressure of experimental oil are 1.4 mPa·s and 11 MPa at formation conditions (70 °C, 18.9 MPa), respectively. The experimental natural gas was compounded and provided by the Huicheng Ruike Company according to associated gas produced in oil wells of the Changqing tight reservoir. The molar proportion of each component is 77.52% for CH_4, 21.47% for C_2H_6, and 1.01% for CO_2.

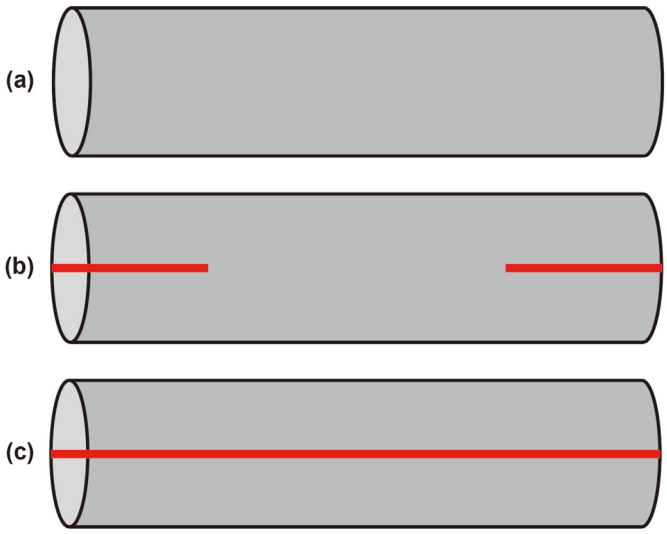

Fig. 1. Schematic diagram of experimental cores. (**a**) Non-fracture core; (**b**) Half-fracture core; (**c**) Penetrating-fracture core.

2.2. Experimental apparatus and procedure

The experimental apparatus for natural gas huff-n-puff was designed and constructed, as shown in Fig. 2. The experimental apparatus consisted of a pressure subsystem, a temperature control subsystem, a high-pressure core holding subsystem, an oil–gas separation subsystem, and an NMR measurement subsystem. Natural gas in the intermediate vessel was injected into the core holder by the displacement pump. The high-pressure core holder was made by Hai'an Company in China. The core holder could withstand up to 50 MPa, which could meet the requirements of the experimental pressure. The oil and gas were produced by adjusting the back pressure regulator (BPR). The temperature control subsystem consisted of a temperature-controlled cabinet and an oven. The oven was used to heat the intermediate vessel. The temperature-controlled cabinet with a control precision of 1 °C was used to heat the core holder. The experiments were conducted at 70 °C. The fluids produced were separated by an oil–gas separator and the produced gases were collected by a draining water gathering gas device. The NMR data could be measured by an NMR apparatus (MacroMR12-150H-VTHP, Niumag Corporation). Since the online NMR apparatus was unable to withstand the high-pressure and high-temperature conditions, the NMR data was obtained offline under laboratory conditions. The process did not affect the accuracy of the test results. The magnetic intensity of the NMR spectrometer is 0.3 ± 0.05 T. The echo and scanning numbers are 18,000 and 32, respectively.

The experimental procedures are as follows.

(1) Core samples were cleaned using a Soxhlet extractor. Then they were dry weighted (m_d) after being put in the oven for 48 h. After vacuuming the core, the oil sample was pumped into the core holder at the injection pressure of 18.9 MPa and the system temperature of 70 °C until the oil was observed at the outlet. After that, the back pressure was set to 18.9 MPa, and the oil was still injected into the core holder until the system pressure reached 18.9 MPa for 2 days to achieve the initial oil saturation (Song et al., 2022b; Yang et al., 2023). The cores were placed in the oven at the temperature of 70 °C for 24 h. Then the oil-saturated cores were weighed (m_s) and scanned by the NMR apparatus. The NMR data before huff-n-puff was obtained.

(2) The natural gas was injected into the intermediate vessel with a pressure of 20 MPa at room temperature. The gas could not be directly pressurized to the experimental pressure due to the gas expansion by heat. Then the intermediate vessel was put in the oven at a temperature of 70 °C.

(3) The core samples were placed in the high-pressure core holder. The temperature-controlled cabinet was set at 70 °C. The connecting line between the intermediate vessel and the core holder was enveloped with a heatproof lagging to reduce heat loss.

(4) In the huff-n-puff experiments, only the left side of the core holder was connected with the intermediate vessel and the oil–gas separator, while the other was blocked. The confining pressure was adjusted to 30 MPa.

(5) The valve (valve 1) connecting the high-pressure core holder and the intermediate vessel was open. The natural gas was injected into the cores at a constant pressure of 26 MPa for 1 h.

(6) The valve 1 was closed and soaking time was maintained to allow the natural gas to dissolve and diffuse for 2 h.

(7) After the soaking stage, the back pressure was adjusted to the designed pressure of 10 MPa by BPR. The valve (valve 2)

Table 1
Basic properties of tight cores.

Core No.	Core length, mm	Core diameter, mm	Core porosity, %	Core permeability, mD	Fracture length, mm	Fracture type
1	130.12	24.86	8.98	0.0349	0	Non-fracture
2	130.16	24.80	9.04	0.0346	65	Half-fracture
3	130.00	24.82	8.93	0.0344	130	Penetrating-fracture

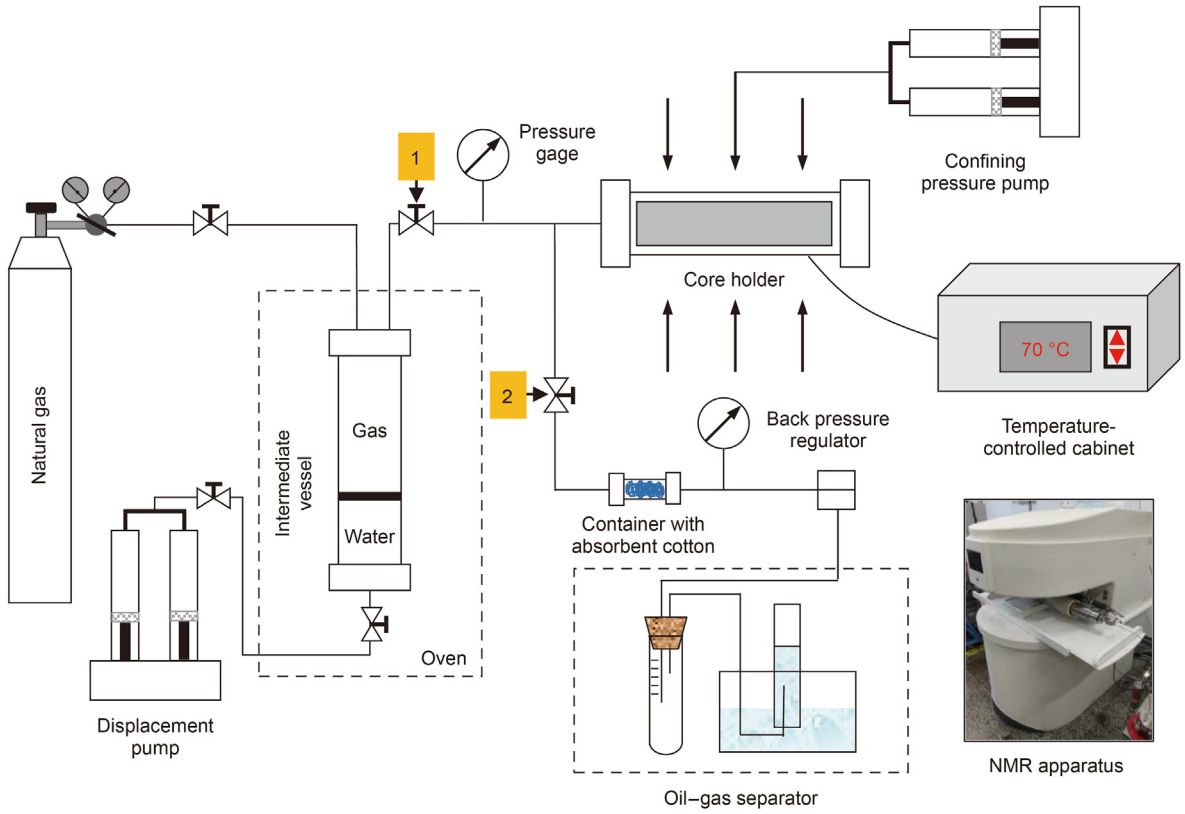

Fig. 2. Schematic diagram of the experimental apparatus for natural gas huff-n-puff.

connecting the core holder and the oil–gas separation device was opened. The container with absorbent cotton was placed at the outlet to collect the oil production.

(8) The experiment was finished after repeating steps (5)–(7) for 3 cycles. The amount of natural gas injected was recorded. The T_2 spectrum for every core after the natural gas huff-n-puff test was measured with NMR apparatus.

Considering that there may be a very small amount of oil in the very short pipelines at the outlet of the core holder, after each huff-n-puff cycle, the short pipelines and the container filled with absorbent cotton were weighed (m_i) by the balance with a control precision of 0.0001 g. Then the accumulative oil recovery is calculated using the following equation.

$$R_i = \frac{m_i - m_o}{m_s - m_d} \times 100\% \quad (1)$$

where R_i is the accumulative oil recovery in cycle i; m_i is the mass of the short pipelines and the container with absorbent cotton in cycle i; m_o is the original mass of the short pipelines and the container with absorbent cotton; m_s is the mass of the oil-saturated core; m_d is the dry mass of the core. The content of saturated oil can be determined by the difference between m_s and m_d. Combined with porosity data, the initial oil saturation of the three tight cores can be calculated to be 91.33%, 92.42%, and 92.23%, respectively.

2.3. Quantitative analysis method of NMR

The T_2 curve of NMR reflects the fluid distribution characteristics in pore spaces. The higher the relaxation time T_2 is, the larger the pore size is. The mercury injection curve can reflect the pore throat structure. The average pore–throat ratio is introduced to establish the relationship between pore radius and pore throat radius. Then a conversion relationship between relaxation time T_2 and pore throat radius can be established (Ding et al., 2018; Huang et al., 2020; Gao et al., 2021). The conversion method is described in detail in our previously published work (Yao et al., 2022). The quantitative conversion relations of relaxation time T_2 and pore throat radius for three cores were established to better investigate the fluid utilization and remaining oil distribution of different pore spaces. The conversion formulas of the non-fracture core, half-fracture core and penetrating-fracture core are shown in Eqs. (2)–(4), respectively. The NMR T_2 spectrum curve was transformed into the pore throat radius distribution curve.

$$r_1 = 0.0401 T_2^{1/2.328} \quad (2)$$

$$r_2 = 0.0246 T_2^{1/2.124} \quad (3)$$

$$r_3 = 0.0258 T_2^{1/2.214} \quad (4)$$

where T_2 is the relaxation time, ms; r_1, r_2, and r_3 are the pore throat radii of the non-fracture core, half-fracture core and penetrating-fracture core , μm.

In addition, the signal peak area corresponding to the relaxation time is proportional to the amount of crude oil in the pores (Huang et al., 2021; Tang et al., 2022). The proportions of different pore spaces can be calculated according to Eq. (5). The pore space distribution was summarized based on the NMR signals of the saturated oil cores. The influence of the fractures on the pore space distribution of the core samples also could be analyzed. It is equally important to analyze the recovery characteristics of oil in different

pore spaces by comparing the NMR results before and after huff-n-puff. Therefore, the contribution percentage of different pore spaces to oil recovery was introduced and calculated according to Eq. (6). Eq. (6) can quantitatively characterize the oil productivity of different pore spaces to determine the pore range conducive to natural gas huff-n-puff. Fig. 3 illustrates the calculation method of pore space proportion and oil recovery contribution for the relaxation time between 4 and 100 ms.

$$P_i = \frac{S_{pi} + S_{ri}}{S_B} \tag{5}$$

$$E_{iC} = \frac{S_{pi}}{S_B - S_A} \tag{6}$$

where P_i is the pore space proportion for relaxation time range i; S_{pi} is the green shadow area surrounded by the black line and the red line for the relaxation time range i; S_{ri} is the blue shadow area surrounded by the red line and the abscissa axis; S_B is the area surrounded by the black line and the abscissa axis for the entire relaxation time range; S_A is the area surrounded by the red line and the abscissa axis for the entire relaxation time range; E_{iC} is the contribution percentage of pore space within relaxation time range i to the total oil recovery.

3. Numerical simulation

The pore-scale oil production characteristics were quantitatively analyzed by NMR data. To further study the performance of natural gas huff-n-puff in tight cores with different fracture lengths, dual-permeability models were established using CMG-GEM based on huff-n-puff experiments. The fluid model was established using the CMG-WINPROP module based on the physical properties of tight oil in the Changqing Formation. The huff-n-puff simulation cases of non-fracture core, half-fracture core, and penetrating-fracture core were conducted. The influence characteristics of important factors on development effects were investigated based on the huff-n-puff simulation models. The injection pressure, soaking time, and diffusion coefficient were selected as important factors to conduct the single-factor analysis. Besides, the sensitivity analysis of the three factors was performed using RSM.

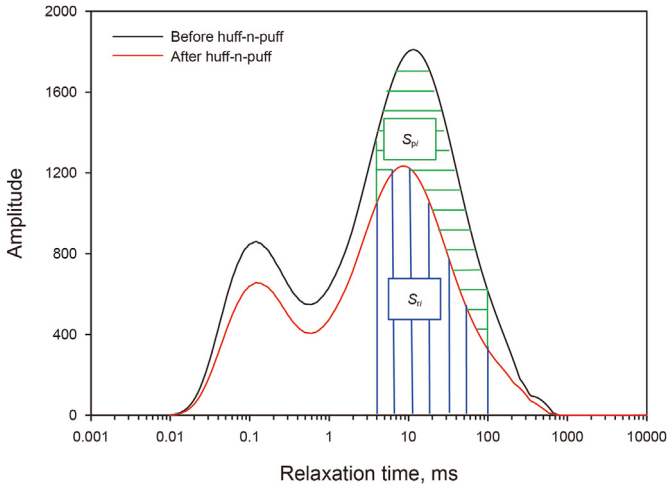

Fig. 3. Calculation diagram of the space proportion and the oil recovery contribution for different pores.

3.1. Simulation model description

The experimental cores were horizontally placed in the high-pressure core holder. The gas was injected and flowed out from one end side of the core during the huff-n-puff process resulting in the linear flow of experimental fluid. The Cartesian simulation model which is better and more convenient to simulate the linear flow was used to simulate the gas huff-n-puff (Yu et al., 2017). The equivalent simulation model was established based on the same cross-sectional area to eliminate the size effect for comparison. The domain with the dimension of 0.13 × 0.022 × 0.022 m was discretized into 26 × 1 × 11 Cartesian grid blocks. Fig. 4 shows the 3-D view of the non-fracture simulation model. A huff-n-puff well was drilled in the center of the left-most side grid in the simulation model. The huff-n-puff well perforated all layers. A single grid block was set up in the Y direction. The purpose was to simulate the uniform contact between the core injection end face and natural gas in the huff-n-puff experiments.

The optimal fluid characterization is essential for the accuracy of numerical simulation. For the compositional simulation, the Peng–Robinson equation of state (PR-EOS) model was constructed in the CMG-WINPROP module using laboratory PVT data. The PVT tests included constant composition expansion (CCE), differential liberation test (DL), swelling test, and separator test. The compositional model performs the material balance equation calculation at each time step. Therefore, to improve the calculation efficiency, the individual components were lumped into seven pseudo components (Shilov et al., 2022). The method of lumping components has been validated by Li and Sheng (2017), and Hamdi et al. (2018). Parameters such as critical temperature, critical pressure, molar weight, and volume shift were tuned to match the PVT data including the saturation pressure, gas–oil ratio, formation volume factor, crude oil density, and relative volume. The Jossi–Stiel–Thodos (JST) viscosity correlation was used to match the crude oil viscosity. The compositions of seven pseudo components and detailed data for the Peng–Robinson EOS are shown in Table 2. Table 3 lists the matching results. The matching errors of the fluid model were all within 2%, indicating that a good agreement between the fluid model and PVT data was obtained. Therefore, it was more convincing to study the mechanism of natural gas huff-n-puff in tight oil cores.

In order to simulate the position and properties of the fractures in cores, the fine grid method and the equivalent method of fracture conductivity were used to establish the fractures in the half-fracture and penetrating-fracture models (Kalra et al., 2018). The fractures were implemented in a middle well perforation plane. The grid step in the K direction is 2 mm, which is set as the equivalent fracture width, thus, the fracture permeability is equivalent to 47.614 mD to ensure the same fracture conductivity. For the half-

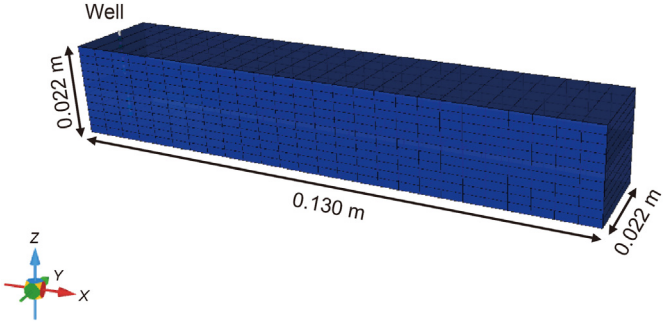

Fig. 4. Three-dimensional diagram of the numerical simulation model.

Table 2
The compositions and properties of pseudo components.

Pseudo component	Mole fraction, mol%	P_c, atm	T_c, K	Acentric factor	MW, g·gmol^{-1}	Volume shift
CO_2	0.17	72.80	304.20	0.2250	44.01	−0.082
N_2	0.37	33.50	126.20	0.0400	28.01	−0.193
CH_4	29.38	45.40	190.60	0.0080	16.04	−0.160
C_2H_6	9.66	48.20	305.40	0.0980	30.07	−0.113
C_3–C_4	17.04	42.58	377.33	0.1657	49.50	−0.091
C_5–C_{10}	18.62	32.21	522.51	0.3303	101.10	0.029
C_{11+}	24.76	13.37	805.70	0.9201	291.29	0.148

Table 3
The matching results of main parameters.

Parameter	Experimental value	Simulative value	Error, %
Saturation pressure, MPa	11	10.922	0.71
Gas–oil ratio (GOR), $m^3 \cdot m^{-3}$	109	111	1.83
Formation volume factor, $rm^3 \cdot sm^{-3}$	1.404	1.393	0.78
Crude oil density, g·cm^{-3} (0.1 MPa, 15.55 °C)	0.8376	0.8384	0.095
Crude oil viscosity, mPa·s (18.9 MPa, 70 °C)	1.40	1.40	0.00

fracture model, the length of both left and right fractures is set to 32.5 mm. For the penetrating-fracture model, all the grids in the middle layer of the model are fracture cells. As the existing number of grids can accurately describe the flow transport in the model, the fracture grid is not refined to improve the calculating speed.

Based on the properties and parameters of the model, the maximum time step size and minimum time step size are adjusted to 0.01 and 1×10^{-12} d, respectively. The normal variation per time step for pressure is controlled to 5000 kPa, and the saturation is 0.001. Set the maximum newton iterations to 12, and turn off the adaptive implicit method. The linear solver precision is 1×10^{-8}, the linear solver factorization is 2, and the number of linear solver iterations is 200. The final simulation model has good convergence and a fast calculation speed.

Then the huff-n-puff simulation schemes of the non-fracture model, half-fracture model, and penetrating-fracture model were designed and conducted. The natural gas huff-n-puff was performed for 3 cycles in each simulation scheme. Table 4 shows the correspondence between the laboratory experiment cores and the simulation models.

3.2. Design of simulation schemes

The single-factor analyses of three factors including injection pressure, soaking time, and diffusion coefficient were separately conducted based on three numerical simulation models. Table 5 lists the simulation schemes where the diffusion coefficient refers to the diffusion coefficient of natural gas in the oil phase obtained experimentally.

Most of the current studies ignore the interaction between the influence factors. The quantitative investigation on the influence degree of the factors is of lack. Therefore, the sensitivity analysis was conducted using RSM to quantitatively investigate the influence of three factors and their interaction on huff-n-puff performance. The injection pressure (A), soaking time (B), and diffusion coefficient (C) were selected as the input variables in the Box-Behnken design which is a common design method used in RSM. The reasonable ranges of three variables were determined based on the single-factor analysis. Three levels were selected within the reasonable range of each variable. Table 6 lists the input variables and levels. The response surface model was designed. In all, 15 experimental points were obtained, in which the zero-point test was repeated three times to estimate the simulation error caused by different iteration time steps. Besides, the oil recovery of ten huff-n-puff cycles was taken as the response value. Three response surface models were designed based on three simulation models. The CMG-GEM module was used to run all simulation schemes.

4. Results and discussion

4.1. The pore-scale oil production characteristics of natural gas huff-n-puff

The pore spaces of core samples were divided into four categories: micro-pores (0.001–0.01 μm), small pores (0.01–0.1 μm), medium pores (0.1–1 μm), and macro-pores (1–10 μm) according to the range of pore throat radius. This process was conducive to study of the characteristics of oil production in different pore spaces. Fig. 5 shows the NMR T_2 distributions of the non-fracture core, half-fracture core, and penetrating-fracture core before and after huff-n-puff. According to the T_2 distribution before huff-n-puff, as shown in the green curve in Fig. 5, the proportion of each pore category was calculated using Eq. (5). According to the NMR T_2 spectrum curves before and after gas huff-n-puff, the contribution percentage of different pore spaces to the oil recovery was calculated using Eq. (6). Table 7 lists the calculation results.

Table 7 shows that the tight cores are mainly composed of medium and small pores, in which the proportions of medium pores are about 60% and those of small pores are more than 30%. The proportions of different pore spaces for the three cores are

Table 4
The correspondence between the experimental cores and simulation models.

Numerical simulation model	Core No. in huff-n-puff experiments	Fracture length
Model 1	Core 1	Non-fracture
Model 2	Core 2	Half-fracture
Model 3	Core 3	Penetrating-fracture

Table 5
The simulation schemes of single-factor analysis.

Parameter	Scheme of simulation	Basic parameter value
Injection pressure, MPa	20, 24, 28, 32, 36	26
Soaking time, h	1, 2, 5, 10, 20	2
Diffusion coefficient, 10^{-5} cm^2/s	0.5, 1.5, 4.5	1.5

Table 6
Three input variables and levels for response surface models.

Factor	Variable	Levels		
		−1	0	1
Injection pressure, MPa	*A*	20	28	36
Soaking time, h	*B*	1	10.5	20
Diffusion coefficient, 10^{-5} cm^2/s	*C*	0.5	1.5	4.5

plotted in Fig. 6. Cores 1, 2, and 3 represented the non-fracture core, half-fracture core, and penetrating-fracture core, respectively, shown in Table 1. It is found that the existence of fractures in the cores mainly increases the proportions of medium and macro-pores. It can be seen from Fig. 5 and Table 7 that the three cores show the same law: the amplitude corresponding to macro-pores and medium pores is significantly reduced, while the signal amplitude corresponding to micro-pores is weakly increased. The oil in medium pores contributes the most to the core oil recovery. The difference was that the overall NMR amplitude of the fractured cores decreased more after natural gas huff-n-puff. The longer the fracture, the greater the decreasing degree of signal amplitude. It means more oil production.

The injected natural gas preferentially entered the macro-pores with lower capillary pressure. Then gas gradually diffused into medium pores, small pores, and micro-pores under pressure and concentration gradients. On the one hand, natural gas carried a small part of crude oil forward. On the other hand, the gas pushed oil into the deeper matrix due to the pressure gradient. Both processes resulted in the increase in crude oil in micro-pores and even small pores. In the puffing stage, gas expansion in crude oil played the role of dissolved gas drive, giving priority to recovering the crude oil in the macro-pores. The crude oil in the medium pores flowed through the macro-pores and was easily developed. However, the crude oil in the micro-pores was difficult to be produced due to the large capillary resistance. The gas huff-n-puff process eventually led to the increase in the T_2 signal amplitude corresponding to the micro-pores. Although the utilization of crude oil in the macro-pores is very large, the contribution percentage of macro-pores to core oil recovery is very small due to the extremely low pore space proportion. The proportion of medium pores is very high, which leads to the biggest contribution to the core oil

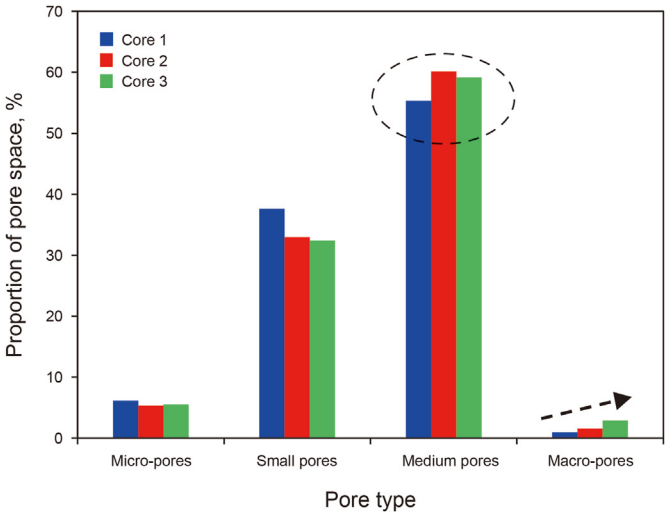

Fig. 6. The proportions of different pore spaces.

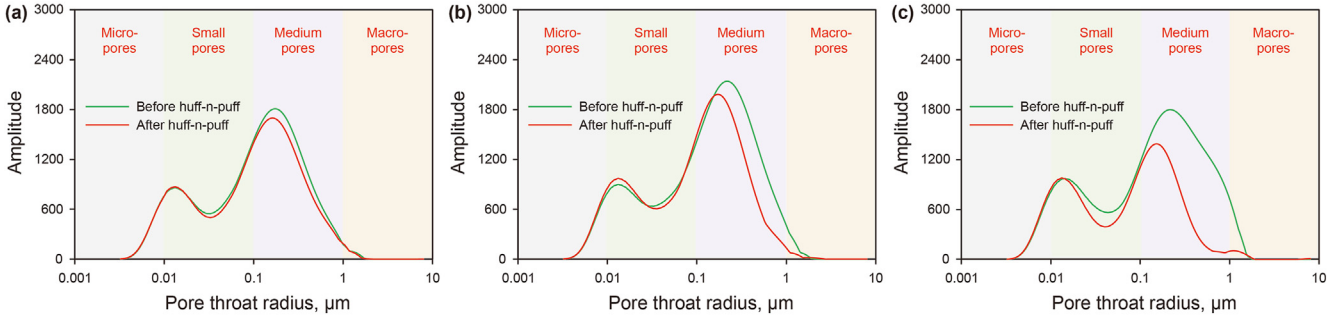

Fig. 5. NMR T_2 distributions before and after natural gas huff-n-puff of (**a**) non-fracture core, (**b**) half-fracture core, and (**c**) penetrating-fracture core.

Table 7
The proportion of different pore spaces and the contribution percentage to oil recovery.

Pore category	The proportion of pore space, %			Contribution percentage of the pore to oil recovery, %		
	Non-fracture core	Half-fracture core	Penetrating-fracture core	Non-fracture core	Half-fracture core	Penetrating-fracture core
Micro-pore	6.12	5.32	5.53	−0.70	−2.31	−0.91
Small pore	37.63	32.97	32.41	19.35	−3.21	10.16
Medium pore	55.31	60.12	59.15	80.09	98.28	84.91
Macro-pore	0.94	1.59	2.91	1.26	7.24	5.84

recovery. The contribution percentages of medium pores are more than 80%. It can be found that smaller pores are unfavorable for natural gas huff-n-puff to improve tight oil recovery. Therefore, volume fracturing is an effective measurement to increase the larger pores to develop tight reservoirs.

Table 8 and Fig. 7 show the cumulative oil recovery and oil exchange ratio of natural gas huff-n-puff in three tight cores, where the oil exchange ratio is defined as the ratio of the produced oil mass to the injected natural gas volume for three cycles. For the non-fracture core, with the increase in huff-n-puff cycles, the increasing extent of oil recovery gradually decreases without an obvious inflection point, and the ultimate oil recovery is 15.4%. For the half-fracture core and penetrating-fracture core, the effective oil production period is mainly the first two cycles, and the curve of cumulative oil recovery slows down from the third cycle. For fractured cores, in the huffing stage, the injected gas preferentially entered the fracture and then penetrated the matrix under the pressure and concentration gradients. Therefore, the longer the fracture, the farther the gas diffusion distance, the larger the contact area of the two-phase, and the stronger the mass transfer effect. In the puffing stage, the crude oil around the fracture was the first to be produced. With the pressure conduction, the crude oil in the matrix was gradually pushed into the fracture and recovered. Therefore, after three huff-n-puff cycles, the fractured cores have greater oil recovery. Moreover, the longer the fracture, the higher the oil recovery and oil exchange ratio.

4.2. Matching experiments

To study the mechanisms of natural gas huff-n-puff and the influence characteristics of important factors using numerical simulation technology, it is necessary to verify the accuracy of the established numerical simulation models. The composition of the injected natural gas in the numerical simulation was the same as that in the experiments. The input parameters, such as the porosity and permeability of the matrix and natural fracture, natural fracture spacing, and the relative permeability curves, were adjusted within a reasonable range to match the experimentally cumulative oil recovery of different cycles (Li and Sheng, 2017). Then the porosities of the matrix and natural fracture were determined to be 9.0% and 0.4%, respectively. The permeabilities of matrix and natural fracture were 0.034 and 10 mD, respectively. Table 9 lists the detailed parameters. The final relative permeability curves after the history matching with the experimental data are presented in Fig. 8 (Wang et al., 2018b; Luo et al., 2022; Shilov et al., 2022). Fig. 9 shows the verification results of the cumulative oil recovery for three simulation models, where the black line represents the positive and negative 5% deviation lines of the experimental values. The errors between the simulation results and experimental values were within 5%. A good agreement between simulation results and experimental results indicated that the numerical simulation cases can characterize the natural gas huff-n-puff in the non-fracture core, half-fracture core, and penetrating-fracture core. It also made good preparation for further mechanism analysis and subsequent sensitivity analysis.

Table 8
The cumulative oil recovery and the oil exchange ratio of natural gas huff-n-puff.

Core No.	Cumulative oil recovery, %			Oil exchange ratio, kg/m^3
	Cycle 1	Cycle 2	Cycle 3	Cycle 3
1	8.5	13.1	15.4	0.81
2	11.1	20.3	21.5	1.15
3	14.3	35.6	40.1	1.70

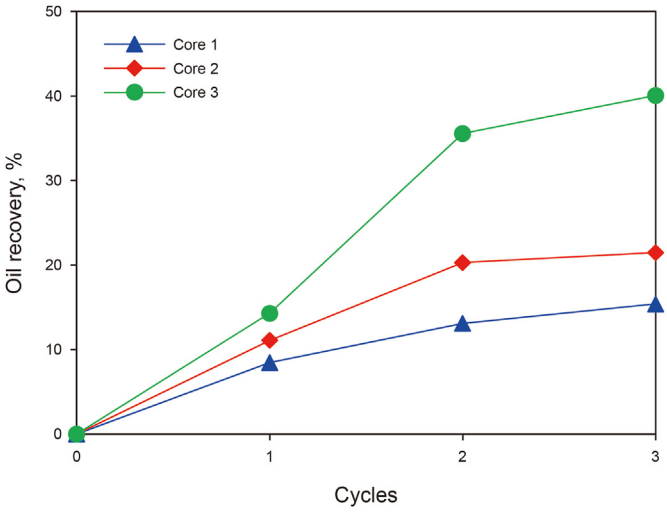

Fig. 7. Cumulative oil recovery of cores with different fracture lengths.

Table 9
The basic parameters of the numerical simulation model.

Parameter	Value
Matrix porosity, %	9.0
Natural fracture porosity, %	0.4
Matrix permeability, mD	0.034
Natural fracture permeability, mD	10
Natural fracture spacing, m	2
Equivalent fracture permeability, mD	47.614
Equivalent fracture width, mm	2
Injection pressure, MPa	26

4.3. The performance of natural gas huff-n-puff

In addition to supplementing formation energy, natural gas dissolves in crude oil, expands crude oil volume, and reduces crude oil viscosity. The reduction of oil viscosity facilitates oil production from the pores and fractures. Natural gas also extracts crude oil components. The mass transfer in two-phase reduces the gas–liquid interfacial tension. The oil production characteristics of different pore spaces were recognized based on the quantitative evaluation of the NMR results above. To further understand the performance of natural gas huff-n-puff, the migration law of GOC, mass transfer characteristics, and the variation of crude oil viscosity in three models were analyzed below.

4.3.1. The migration law of GOC

Considering the position of the fractures, the middle layer grids (from {1 1 6} to {26 1 6}) of the simulation model were selected as the analysis objects. The dimensionless distance was used to quantify the performance of natural gas huff-and-puff. The left-most grid block {1 1 6} is the origin, and the right-most grid block {26 1 6} is the dimensionless distance of 1, as shown in the red grids in Fig. 10. According to the distribution of gas saturation and oil saturation, the position of the GOC at the end of each soaking cycle can be determined, as shown in Fig. 11, where the black surfaces represent the GOC. For the non-fracture model and penetrating-fracture model, the GOC positions were defined by the dimensionless distances between the sixth layer grid of the interface and the origin, as shown in Fig. 11 (e.g. 1). However, since the half-fracture model had two fractures, there were two gas–oil contacts. The dimensionless distance between the sixth layer grid of the left interface and the origin was recorded, which was the left

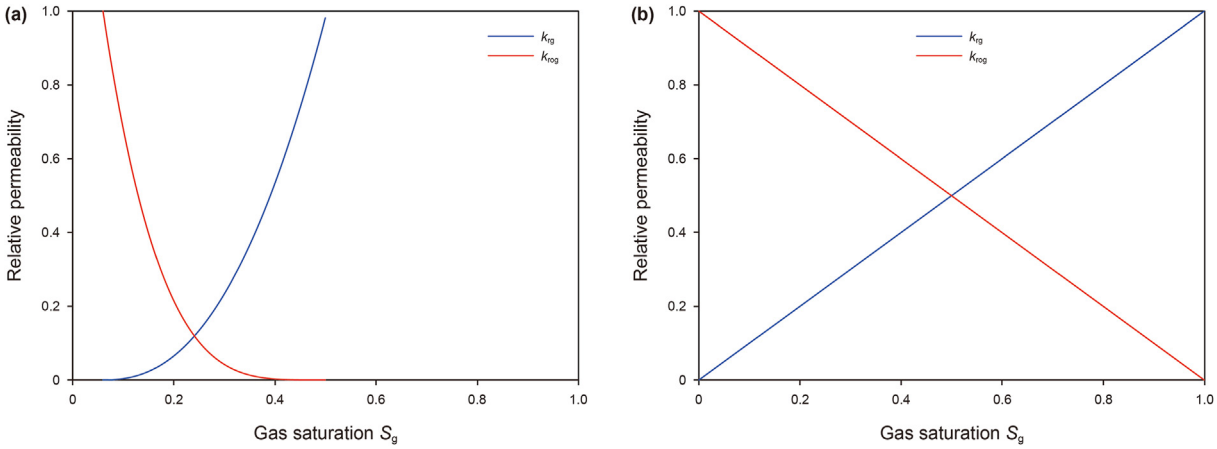

Fig. 8. Relative permeability curves used in the simulation model for (**a**) the matrix and (**b**) the fractures.

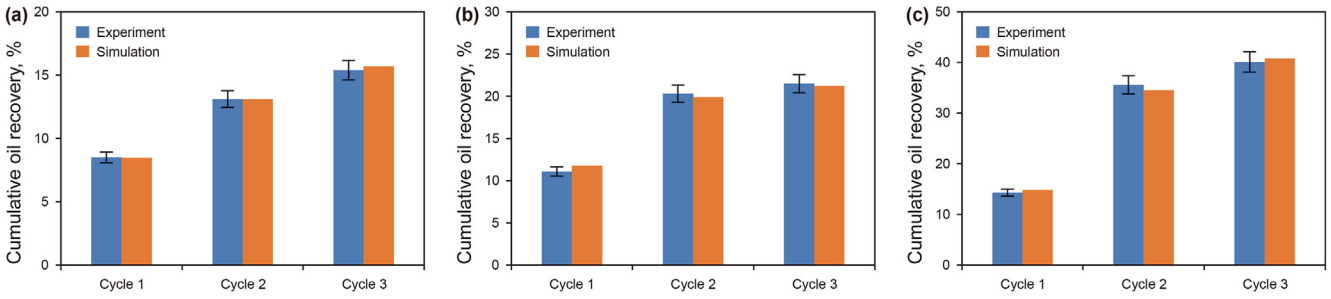

Fig. 9. Verification results for (**a**) non-fracture model, (**b**) half-fracture model, and (**c**) penetrating-fracture model.

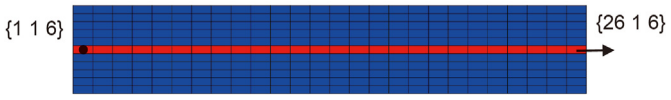

Fig. 10. Schematic diagram of quantitative characterization for natural gas huff-n-puff.

GOC position. The right GOC position was counted with the dimensionless distance between the middle layer grid of the right interface and the grid block {26 1 6}, as shown in Fig. 11 (e.g. 2). Table 10 lists the positions of the GOC in three models at different soaking cycles.

For the non-fracture model, all injected gas dissolved in the oil at the first soaking cycle, causing the GOC to stay at the origin. As the number of huff-and-puff cycles increased, more natural gas was injected, the gas gradually diffused, and the GOC migrated forward. This migration law could also be summarized by the position change of the GOC in the half-fracture model and the penetrating-fracture model. In addition, since the injected gas first was transported through the fracture, the distance range occupied by the gas phase increased as the fracture length increased. For example, the GOC of the non-fracture model only reached the dimensionless

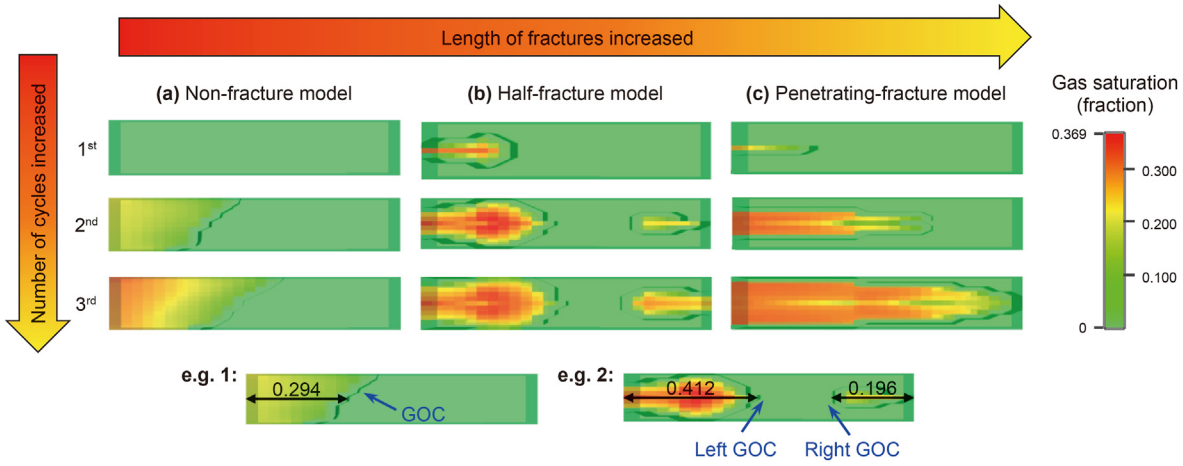

Fig. 11. The diagram of GOC migration in three models.

Table 10
GOC positions in three models at different soaking cycles.

Huff-n-puff cycle	GOC positions (the dimensionless distance)			
	Model 1	Left of model 2	Right of model 2	Model 3
1st cycle	0	0.255	0	0.216
2nd cycle	0.294	0.412	0.196	0.569
3rd cycle	0.412	0.451	0.235	0.961

distance of 0.412 in the third soaking cycle, while the GOC of the penetrating-fracture model reached the dimensionless distance of 0.961. This means that almost the entire length of the penetrating-fracture model was full of the natural gas phase.

4.3.2. Mass transfer in oil and gas phases

Mass transfer between crude oil and natural gas consists of two processes. On the one hand, natural gas is dissolved in crude oil. On the other hand, natural gas extracts lighter components from crude oil. These two mechanisms significantly affect the miscibility of the oil and gas phases and enhance oil recovery.

Considering the composition of injected natural gas, the dissolving mechanism was analyzed with the mole fractions of CH_4 and CO_2 in the oil phase at the end of each soaking cycle. Fig. 12 compares the change curves of CH_4 and CO_2 mole fractions for three models at different soaking cycles. The blue line, green line, and red line represent the first, second, and third natural gas huff-n-puff cycles, respectively. The black dashed lines represent the original mole fractions of the components.

For the non-fracture model, the injected gas first accumulated around the well, then dissolved and diffused into the crude oil near the well. It caused the CH_4 and CO_2 contents in the crude oil to be higher than the original contents, as shown in the blue line above the black dashed line in Fig. 12(a). On the one hand, natural gas diffused further as a gas phase under the pressure and concentration gradients. On the other hand, CH_4 and CO_2 components dissolved in the oil phase were transferred forward. Both diffusion processes resulted in CH_4 and CO_2 contents in the oil phase decreasing as the distance from the well point increased, as shown in the blue line in Fig. 12(a). Considering that there was no GOC at the first cycle, it could be concluded that the injected gas was all dissolved in crude oil. CH_4 and CO_2 components swept to a dimensionless distance of 0.5, where this dimensionless distance was defined as the position of the components' sweep front. As the number of huff-n-puff cycles increased, more gas was injected, the gas spread farther, and more gas was dissolved in the crude oil. As can be seen from the green line in Fig. 12(a), the injected gas could sweep to the dimensionless distance of 0.8 at the second cycle. Combined with the GOC position (the dimensionless distance of 0.294) at the second cycle, the green line displayed that the CH_4 and CO_2 mole fractions in the oil phase remained at a high level within the GOC. The reason may be that the mass transfer in two phases reaches a dynamic equilibrium and the dissolved natural gas content in the crude oil reaches saturation. At the third cycle, the components almost swept through the entire model and the GOC moved to a dimensionless distance of 0.412, as shown in the red line in Fig. 12(a).

Fig. 12(b) shows the variation characteristics of CH_4 and CO_2 contents in the oil phase for the half-fracture model. The injected natural gas first entered and accumulated in the fractures. The process caused natural gas dissolved in crude oil near the fractures to reach saturation at the early stage of huff-n-puff. For example, the components could penetrate as far as the dimensionless distance of 0.39 and reach saturation within the dimensionless distance of 0.255 at the first cycle. With the increase in huff-n-puff cycles, the injected gas gradually diffused and finally broke through to the right fracture. Therefore, the mole fractions of CH_4 and CO_2 in crude oil from both the left and right fractures were high. The CH_4 and CO_2 contents in the oil phase from the middle distance were low, presenting a 'U' curve. Moreover, with the increase in huff-n-puff cycles, the U-shaped region gradually decreased.

Fig. 12(c) shows the mole fractions of CH_4 and CO_2 in the oil

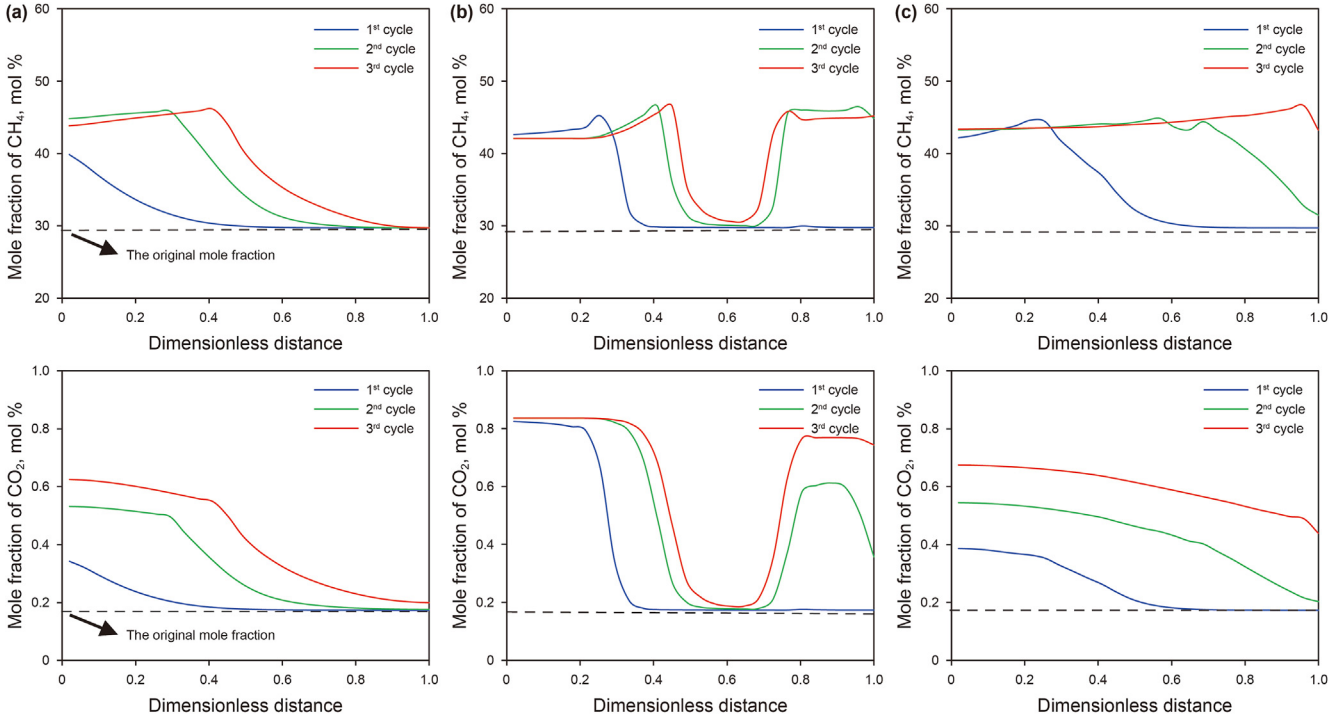

Fig. 12. The mole fractions of CH_4 and CO_2 in the oil phase for (**a**) non-fracture model, (**b**) half-fracture model, and (**c**) penetrating-fracture model.

phase for the penetrating-fracture model. Injected natural gas had a longer penetration depth and the swept front of the components was up to the dimensionless distance of 0.63 at the first cycle. At the second cycle, the components spread through the entire model. At the third cycle, the mole fractions of CH_4 and CO_2 in crude oil remained high throughout the model. It means that the mass transfer between the oil and gas phases reached saturation for almost the entire model, which could be proved by the GOC position (the dimensionless distance of 0.961) of the third cycle.

In addition, the grouped carbon number distributions of the gas phase at the end of each soaking cycle were analyzed to explore the extraction characteristics. The extraction law was similar in the dimensionless length of the model. The composition distributions of C_3–C_4, C_5–C_{10}, and C_{11+} in the gas phase of block {6 1 6} are shown in Fig. 13. Because the natural gas was completely dissolved in crude oil during the first soaking stage, the dimensionless length for the non-fracture model contains no gas phase. Fig. 13 shows the hydrocarbon distributions of the gas phase at the second and third soaking cycles in the non-fracture model. It can be seen that the injected natural gas extracts the light components from crude oil, mainly including C_3–C_4 and C_5–C_{10} components. Due to the extraction mechanism of natural gas, the produced oil is lighter than crude oil, and the remaining oil will become heavier and more difficult to be extracted. Therefore, with the increase in huff-n-puff cycles, the component content extracted by natural gas decreases. Compared with the non-fracture and half-fracture models, this law is more significant in the penetrating-fracture model.

4.3.3. The law of oil viscosity reduction

Fig. 14 shows the changes in crude oil viscosity for three models, and the black dashed line represents the original value. Since the injected gas was dissolved in crude oil, the volume of crude oil expanded, reducing the oil viscosity. Therefore, the decrease in oil viscosity depends on the amount of natural gas components dissolved in the oil phase. The viscosity reduction characteristic is the same as the change law of natural gas component contents in the oil phase. In addition, dissolved CO_2 is more beneficial to the reduction in oil viscosity (Burrows et al., 2020). But the content of CO_2 in natural gas is much lower than that of CH_4. Therefore, it can be found that the curve of the oil viscosity reduction and the change curve of the CH_4 mole fraction in the oil phase maintain a high degree of consistency by comparing Figs. 12 and 14.

4.4. Single-factor analysis

4.4.1. Effect of injection pressure

Fig. 15 shows the oil recovery and oil exchange ratio after ten huff-n-puff cycles under different injection pressures. Fig. 16 presents the interfacial tension at the 3rd, 5th, and 10th soaking cycles in the block {1 1 6}. The three models show the same law. With the increase in injection pressure, the mass transfer effect strengthens, the interfacial tension of the two phases decreases, and the oil recovery is enhanced. Under higher injection pressure, more natural gas is injected, but the corresponding oil production increment is not achieved. Therefore, the oil exchange ratio decreases, as shown in the red line in Fig. 15. In addition, with the increase in huff-n-puff cycles, the contents of the lighter components in the remaining oil were less due to the gas extraction, and the oil properties became worse, leading to increasing interfacial tension between the oil and gas phases.

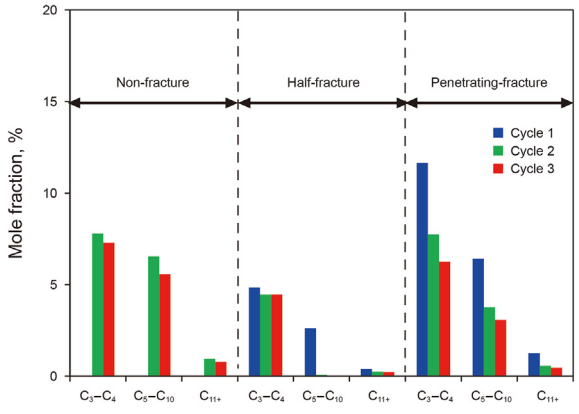

Fig. 13. Grouped carbon number distributions of the gas phase.

4.4.2. Effect of soaking time

The cumulative oil recovery of ten huff-n-puff cycles and its growth rate were selected as the evaluation factors, where the growth rate was defined as the ratio of the difference between oil recovery at two soaking times to the difference between the soaking times (Huang et al., 2022). Fig. 17 illustrates the influence of the soaking time on the oil recovery and the growth rate. Three models all show that the oil recovery increases gradually with the growth of the soaking time, and the growth rate decreases.

For the non-fracture model, the injected gas diffuses slowly. With the increase in the soaking time, the diffusion distance of natural gas was longer and the oil recovery was higher. The curve of the growth rate decreased evenly overall. The growth rate was lower than 0.1 h^{-1} when the soaking time was 20 h. It is considered that the optimal soaking time for the non-fracture model is 20 h. For the half-fracture model and penetrating-fracture model with higher permeability, the volume of the injected gas sweep was larger, and the two phases achieved dynamic equilibrium faster. Therefore, the growth rate of oil recovery dropped significantly. There was a turning point when the soaking time was 10 h. The growth rate was low and did not change much when the soaking time was longer than 10 h. Therefore, 10 h is the best soaking time for fractured models.

4.4.3. Effect of the gas diffusion coefficient

Fig. 18 shows the variation curves of CH_4 mole fraction in the oil phase under different diffusion coefficients (D_e). Fig. 19 shows the oil recovery under different diffusion coefficients. In the case of the same volume of total injected gas, the dissolution rate of natural gas in crude oil was greater when the diffusion coefficient was larger. After the injected gas was dissolved in crude oil, CH_4 in the oil phase diffused forward under the concentration gradient. With the increase in the diffusion coefficient, the variation curves of CH_4 content in the oil phase with distance were flatter, the range of crude oil production was wider, and the oil recovery was higher. The smaller the diffusion coefficient, the steeper the curve. The results are consistent with those presented by Li et al. (2018). Compared with the case without considering the diffusion coefficient, the oil recovery was significantly improved considering the diffusion effect. Of course, it is necessary to consider the diffusion coefficient to better simulate the huff-n-puff process. However, the increase in the oil recovery for the huff-n-puff single-cycle was small as the diffusion coefficients increased. The oil recovery of the penetrating-fracture model was taken as an example, as shown in the black dashed line in Fig. 19. Similar findings are also documented in the literature (Peng and Sheng, 2023).

4.5. Sensitivity analysis

The simulation results of the response surface designs for non-fracture, half-fracture, and penetrating-fracture models are listed in

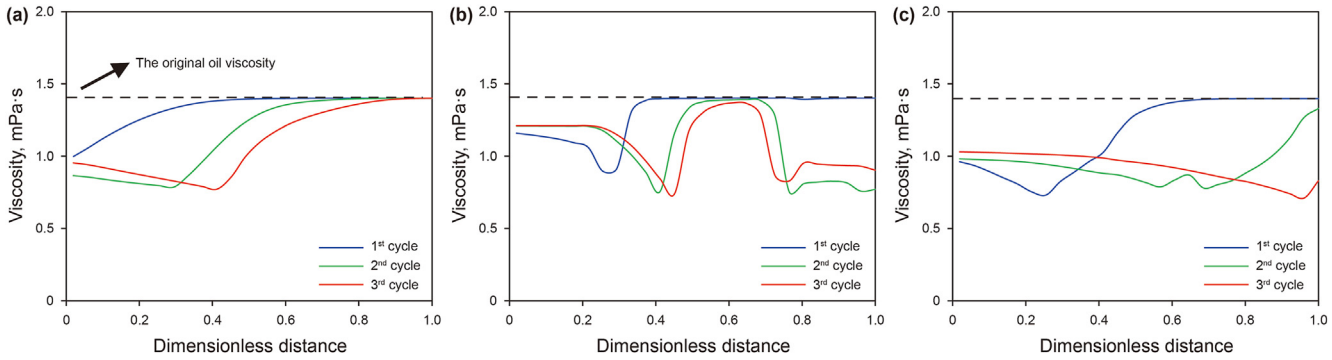

Fig. 14. Change curves for oil viscosity of (**a**) non-fracture model, (**b**) half-fracture model, and (**c**) penetrating-fracture model.

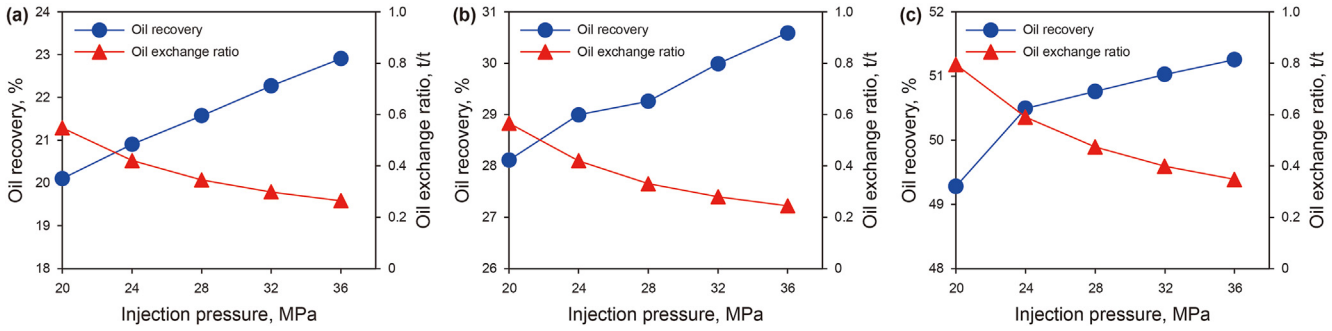

Fig. 15. Oil recovery and oil exchange ratio under different injection pressures of (**a**) non-fracture model, (**b**) half-fracture model, and (**c**) penetrating-fracture model.

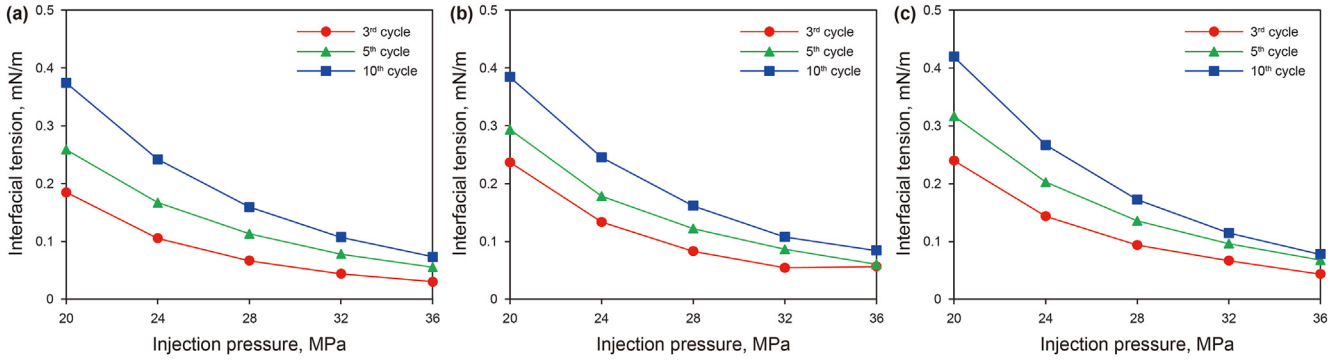

Fig. 16. Effect of injection pressure on interfacial tension for (**a**) non-fracture model, (**b**) half-fracture model, and (**c**) penetrating-fracture model.

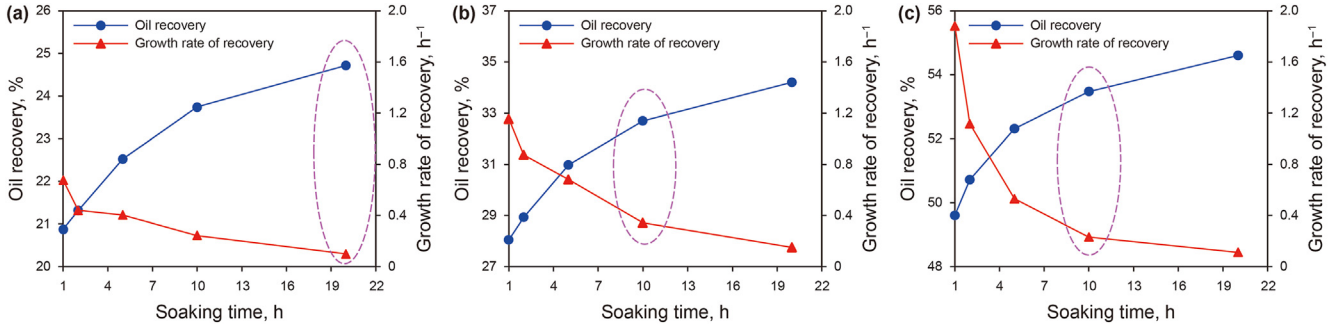

Fig. 17. Effect of soaking time on oil recovery and the growth rate of recovery for (**a**) non-fracture model, (**b**) half-fracture model, and (**c**) penetrating-fracture model.

Appendix A. Based on actual parameters and all simulation results, the RSM method will first attempt to fit the linear relationship between the oil recovery and uncertain parameters. If there is a nonlinear relationship between the parameters and the objective function, a quadratic term will be introduced. If the effect of altering two parameters at the same time on the oil recovery is stronger

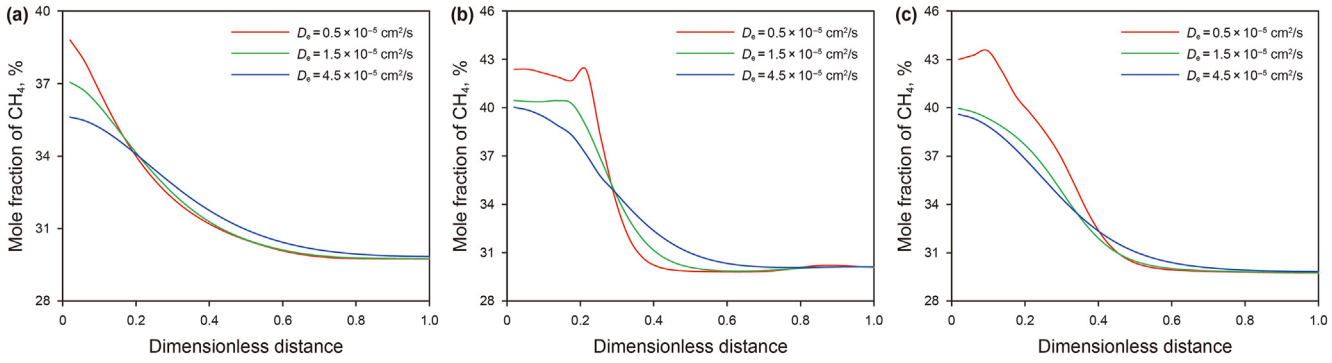

Fig. 18. Changes of CH_4 mole fraction in the oil phase under different diffusion coefficients for (**a**) non-fracture model, (**b**) half-fracture model, and (**c**) penetrating-fracture model.

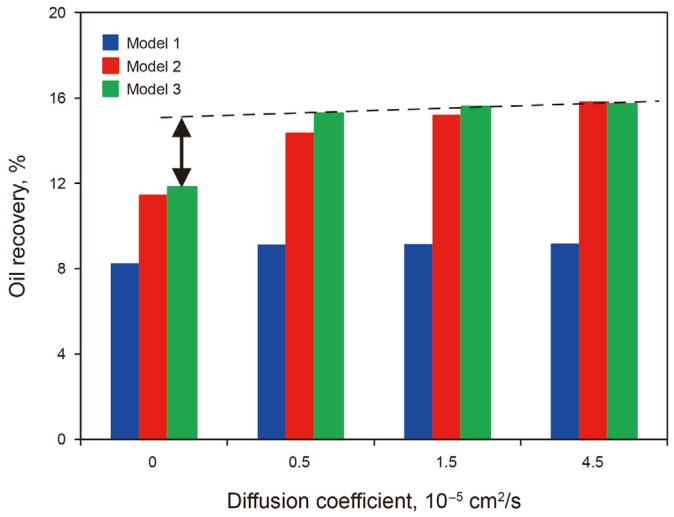

Fig. 19. Effect of diffusion coefficient on oil recovery of natural gas huff-n-puff.

than the sum effects of their respective linear or quadratic terms, the two-factor interaction term will be used to define the relationship with the oil recovery (Kalra et al., 2018). Therefore, three oil recovery response equations, including Y_1 for the non-fracture model, Y_2 for the half-fracture model, and Y_3 for the penetrating-fracture model, were finally fitted, which contained the linear, quadratic, and two-factor interaction terms of uncertain parameters and the coefficients of these terms. The equations fitted to the oil recovery response surface in terms of actual factors, and variance analysis are presented in Appendix B. The scatter plots of actual and predicted values for the three models are shown in Fig. 20. The obtained *P*-values for the three response surface models are all lower than 0.01. The results indicate that the regression models are highly reliable and that all factors are beneficial to the prediction power of the models. The non-fracture response model was taken as an example to illustrate the accuracy. The '*R*-squared' (R^2), 'Adjusted *R*-squared' (R^2_{Adj}), and 'Predicted *R*-squared' (R^2_{Pre}) of the non-fracture regression model were 0.9745, 0.9286, and 0.8378, respectively. The high R^2 and the reasonable difference between R^2_{Adj} and R^2_{Pre} both indicated that the quadratic polynomial models had high accuracy and predictive capability. The same is true for half-fracture and penetrating-fracture regression models. The good match between actual and predicted values also supported this statement, as shown in Fig. 20.

For Y_1, the *P*-values of *A*, *B*, A^2, and B^2 were lower than the significance level of 0.05, indicating that these terms were significant. For Y_2, *A*, *B*, and the two-factor interaction term *AC* were significant. For Y_3, *A*, *C*, the two-factor interaction term *AC*, and the quadratic term A^2 had a significant influence on the oil recovery. The higher *F*-value means that the influence degree of the factor on the response value is greater (Afari et al., 2022). Therefore, according to the *F*-values of the three models, the order of the factors affecting oil recovery could be obtained, as shown in Fig. 21. For the non-fracture and half-fracture models, the injection pressure is the most significant parameter, and the second-most significant parameter is soaking time. The next important parameters in the rank are the interaction between injection pressure and diffusion coefficient, followed by the diffusion coefficient. For the penetrating-fracture model, the most significant parameter is injection pressure. The second-most significant parameter is the diffusion coefficient. The third-most significant term is the interaction between injection pressure and diffusion coefficient. The next important term in the rank is soaking time.

Since the interaction of injection pressure and diffusion coefficient has important effects on the oil recovery for three models, the response surface plots of oil recovery against injection pressure and diffusion coefficient are drawn, as shown in Fig. 22. For the three response models, injection pressure always had a positive effect on oil recovery, which was the same as the law obtained by single-factor analysis. Existing studies have also proven the findings (Song and Yang, 2017; Shilov et al., 2022).

For the non-fracture response model, the oil recovery was greater when the injection pressure and the diffusion coefficient were higher, as shown in Fig. 22(a). The higher density of contour lines in a certain direction indicates that the influence of this factor in the interaction on the response value was greater (Wang et al., 2022). The density of contour lines in the direction of injection pressure is greater than that in the direction of diffusion coefficient, as shown in the contour plot in Fig. 22(a). Therefore, oil recovery is more sensitive to the injection pressure than the diffusion coefficient. For half-fracture and penetrating-fracture response models, when the injection pressure is low, the diffusion coefficient shows a negative effect on the response value, as shown in Fig. 22(b) and (c). When the injection pressure is high, the diffusion coefficient shows a positive effect. The reason may be the mutual restriction of repressurization and the mass transfer mechanism. The higher diffusion coefficient made the gas dissolve more in the crude oil when the injection pressure was low. It caused the pressure supplement to the fractured model to be smaller and the effective production pressure difference was low. Eventually, the oil recovery was reduced. However, when the injection pressure was high, the model had a sufficient pressure supplement. In the meantime, the increased diffusion coefficient was conducive to the mass transfer between the oil and gas phases. The oil recovery was enhanced under the superposition effects of two mechanisms. Similar findings have also been documented in the literature (Sun et al., 2019;

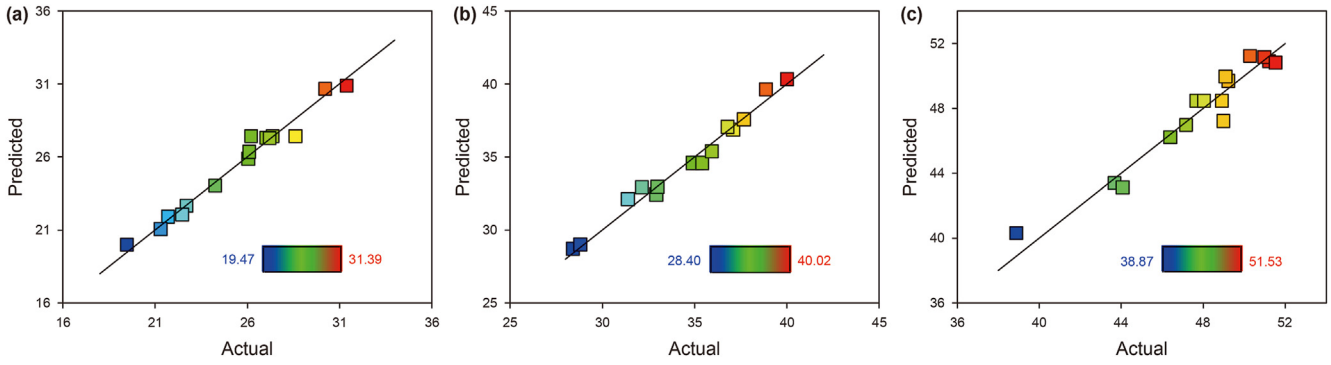

Fig. 20. Model validation for (**a**) non-fracture model, (**b**) half-fracture model, and (**c**) penetrating-fracture model.

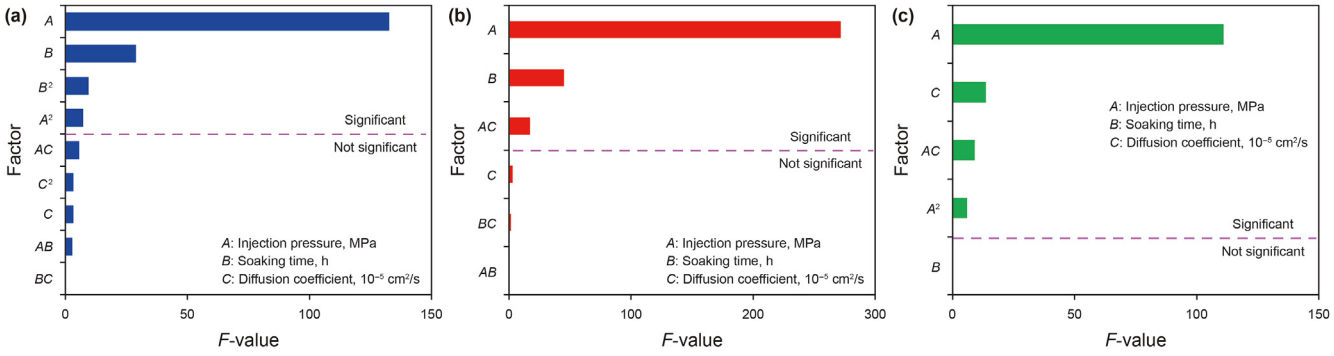

Fig. 21. Ranking of the factors influencing oil recovery for (**a**) non-fracture model, (**b**) half-fracture model, and (**c**) penetrating-fracture model. *A*: Injection pressure, MPa; *B*: Soaking time, h; *C*: Diffusion coefficient, 10^{-5} cm^2/s.

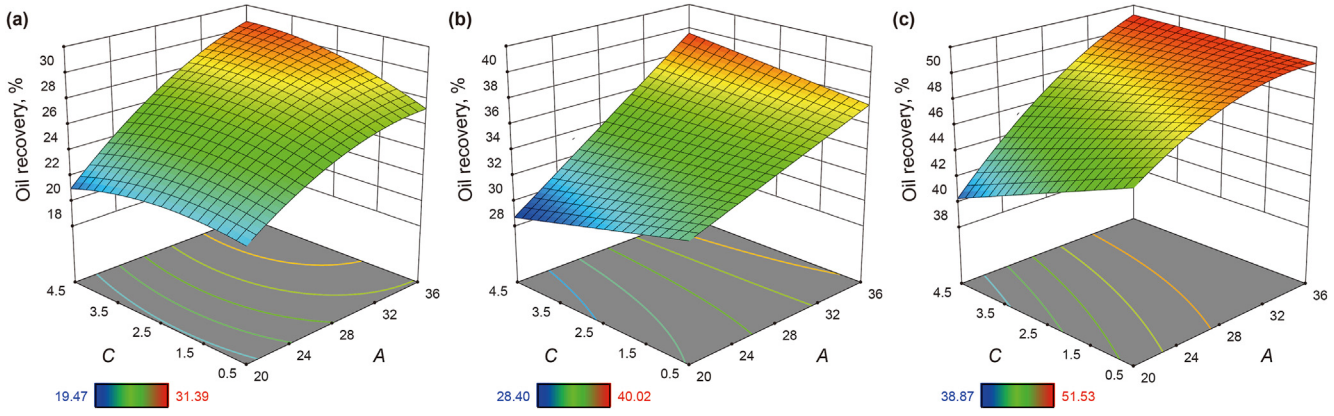

Fig. 22. Three-dimensional response surface plots of interaction between injection pressure (*A*) and diffusion coefficient (*C*) for (**a**) non-fracture model, (**b**) half-fracture model, and (**c**) penetrating-fracture model.

Fu et al., 2021; Peng and Sheng, 2023). In addition, the color of response surfaces in the half-fracture model was richer than that in the penetrating-fracture model at high injection pressure. It indicated that with the increase in fracture length, the sensitivity of oil recovery to diffusion coefficient decreased at high injection pressure. Therefore, in tight oil reservoir exploitation, the combined effects of gas injection pressure and diffusion should be considered to determine the huff-n-puff parameters to maximize oil recovery.

5. Conclusions

Three cores with different fracture lengths were made, including non-fracture, half-fracture, and penetrating-fracture cores. Natural gas huff-n-puff experiments in the three cores were conducted with the gas huff-n-puff experimental device. The microscopic characteristics of oil production in different pore spaces were quantitatively analyzed by using the NMR T_2 spectrum. According to the huff-n-puff experiments, three core-scale numerical simulation models were established and calibrated. Then the performance evaluation of natural gas huff-n-puff and single-factor analysis were conducted. Finally, the sensitivity analysis was performed using RSM. The main conclusions are as follows.

(1) Tight cores mainly consist of medium pores (0.1–1 μm) and small pores (0.01–0.1 μm). The fracture mainly increases the proportion of macro-pores (1–10 μm) and medium pores.

Regardless of whether it is a non-fracture core, half-fracture core, or penetrating-fracture core, the crude oil in the macropores and medium pores is mainly produced after natural gas huff-n-puff for three cycles. The oil production in the medium pore contributes the most to tight oil recovery. It seems that smaller pores are unfavorable for natural gas huff-n-puff. Volume fracturing is an effective measurement to increase the larger pores to develop tight reservoirs.

(2) With the increase in huff-n-puff cycles, the oil and gas two phases contact and the components sweep front migrate deeper. The contents of CH_4 and CO_2 in the oil phase remain at a high level within the GOC, while between the GOC and the components sweep front, the contents of CH_4 and CO_2 decrease with the increase in the dimensionless distance due to molecular diffusion. The gas component sweep volume is higher with the increase in fracture length. The injected natural gas extracts the light components from crude oil, mainly including C_3–C_{10} components. In addition, the reduction law of oil viscosity is consistent with the change law of CH_4 content in the oil phase.

(3) With the increase in injection pressure, the interfacial tension between the oil and gas phases decreases, and the oil recovery is improved. The soaking time required for fractured models is shorter than that for non-fracture models. With the increase in diffusion coefficient, the variation curve of CH_4 content in the oil phase with dimensionless distance was flatter, and the oil recovery of a single huff-n-puff cycle was weakly enhanced. Therefore, the gas injection pressure can be maximized and the soaking time for huff-n-puff in tight reservoirs after fracturing should be shortened appropriately.

(4) Compared with soaking time and diffusion, the injection pressure is the most significant factor underlying the recovery of natural gas huff-n-puff in matrix-fracture cores. Besides the influence of single-factor, the interaction effects of gas injection pressure and diffusion also should be considered in the natural gas huff-n-puff implementation of tight reservoirs after fracturing.

Declaration of competing interest

The authors declare that they have no known competing financial interests or personal relationships that could have appeared to influence the work reported in this paper

Acknowledgments

This research was supported by the National Natural Science Foundation of China (Grant No. U22B6004, 51974341, 51904324), the Fundamental Research Funds for the Central Universities (No. 20CX06070A), and the Science and Technology Support Plan for Youth Innovation of University in Shandong Province (Grant No. 2019KJH002). We also appreciate the reviewers and editors for their constructive comments to make the paper high quality.

Appendix A. The response results for non-fracture, half-fracture, and penetrating-fracture response models

Table A1
The response results for three response surface models.

Run	Injection pressure, MPa	Soaking time, h	Diffusion coefficient, 10^{-5} cm^2/s	Oil recovery, %		
				Model 1	Model 2	Model 3
1	36	1	2.5	26.07	37.10	51.22
2	20	20	2.5	21.71	31.39	43.68
3	28	1	0.5	22.71	32.15	49.23
4	36	20	2.5	31.39	40.02	50.99
5	28	10.5	2.5	26.21	35.15	47.68
6	28	20	0.5	26.10	36.80	49.09
7	36	10.5	4.5	30.21	38.89	50.29
8	28	10.5	2.5	28.62	34.92	48.92
9	20	10.5	4.5	21.31	28.40	38.87
10	36	10.5	0.5	27.04	37.68	51.53
11	28	10.5	2.5	27.38	35.43	48.05
12	20	10.5	0.5	22.48	32.94	46.40
13	28	20	4.5	27.21	35.94	48.99
14	28	1	4.5	24.27	33.00	47.18
15	20	1	2.5	19.47	28.82	44.07

Appendix B. Regression fitting results of the sample data for non-fracture, half-fracture, and penetrating-fracture models

Eqs. (B.1) to (B.3) provide the equations fitted to the oil recovery response surface in terms of actual factors. Tables B1 to B3 list the variance analysis of quadratic equations for the non-fracture model, half-fracture model, and penetrating-fracture model, respectively.

where Y_1, Y_2, and Y_3 are the oil recovery factors of non-fracture, half-fracture, and penetrating-fracture models, respectively; A is injection pressure, B is soaking time, and C is diffusion coefficient.

$$Y_1 = 0.531349 + 1.30649A + 0.254263B - 0.466754C + 0.010143AB + 0.067895AC - 0.005876BC - 0.019967A^2 - 0.016227B^2 - 0.216149C^2 \quad \text{(B1)}$$

$$Y_2 = 25.27665 + 0.265185A + 0.195330B - 2.48934C + 0.001168AB + 0.089852AC - 0.022388BC \quad \text{(B2)}$$

$$Y_3 = 27.18808 + 1.39130A + 0.013711B - 3.43336C + 0.098277AC - 0.020581A^2 \quad \text{(B3)}$$

Table B1
Variance analysis of quadratic equations for non-fracture model.

Source	Sum of squares	Degree of freedom	Mean square	*F*-value	*P*-value
Model	159.13	9	17.68	21.22	0.0018
A	110.50	1	110.50	132.62	<0.0001
B	24.12	1	24.12	28.95	0.0030
C	2.73	1	2.73	3.27	0.1303
AB	2.38	1	2.38	2.85	0.1520
AC	4.72	1	4.72	5.67	0.0632
BC	0.0499	1	0.0499	0.0598	0.8165
A^2	6.03	1	6.03	7.24	0.0433
B^2	7.92	1	7.92	9.50	0.0274
C^2	2.76	1	2.76	3.31	0.1284
Lack of fit	1.24	3	0.4148	0.2839	0.8368

$R^2 = 0.9745$, $R^2_{Adj} = 0.9286$, $R^2_{Pre} = 0.8378$.

Table B2
Variance analysis of quadratic equations for half-fracture model.

Source	Sum of squares	Degree of freedom	Mean square	*F*-value	*P*-value
Model	160.86	6	26.81	56.46	<0.0001
A	129.07	1	129.07	271.82	<0.0001
B	21.38	1	21.38	45.02	0.0002
C	1.39	1	1.39	2.93	0.1252
AB	0.0315	1	0.0315	0.0664	0.8031
AC	8.27	1	8.27	17.41	0.0031
BC	0.7238	1	0.7238	1.52	0.2520
Lack of fit	3.66	6	0.6107	9.07	0.1026

$R^2 = 0.9769$, $R^2_{Adj} = 0.9596$, $R^2_{Pre} = 0.9073$.

Table B3
Variance analysis of quadratic equations for penetrating-fracture model.

Source	Sum of squares	Degree of freedom	Mean square	*F*-value	*P*-value
Model	151.54	5	30.31	28.00	<0.0001
A	120.17	1	120.17	111.02	<0.0001
B	0.1357	1	0.1357	0.1254	0.7314
C	14.87	1	14.87	13.74	0.0049
AC	9.89	1	9.89	9.14	0.0144
A^2	6.48	1	6.48	5.98	0.0370
Lack of fit	8.94	7	1.28	3.19	0.2594

$R^2 = 0.9396$, $R^2_{Adj} = 0.9060$, $R^2_{Pre} = 0.7493$.

References

Afari, S., Ling, K., Sennaoui, B., et al., 2022. Optimization of CO_2 huff-n-puff EOR in the Bakken Formation using numerical simulation and response surface methodology. J. Petrol. Sci. Eng. 215, 110552. https://doi.org/10.1016/j.petrol.2022.110552.

Alharthy, N., Teklu, T., Kazemi, H., et al., 2018. Enhanced oil recovery in liquid-rich shale reservoirs: laboratory to field. SPE Reservoir Eval. Eng. 21 (1), 137–159. https://doi.org/10.2118/175034-PA.

Alzobaidi, S., Kortunov, P., Chhatre, S., et al., 2022. Experimental evaluation of Huff and Puff EOR mechanisms in unconventional rock. In: SPE/AAPG/SEG Unconventional Resources Technology Conference. https://doi.org/10.15530/urtec-2022-3719062.

Burrows, L.C., Haeri, F., Cvetic, P., et al., 2020. A literature review of CO_2, natural gas, and water-based fluids for enhanced oil recovery in unconventional reservoirs. Energy Fuel. 34 (5), 5331–5380. https://doi.org/10.1021/acs.energyfuels.9b03658.

Carlsen, M., Whitson, C., Dahouk, M.M., et al., 2019. Compositional tracking of a huff-n-puff project in the Eagle Ford. In: SPE/AAPG/SEG Unconventional Resources Technology Conference. https://doi.org/10.15530/urtec-2019-539.

Ding, B., Luo, J., Geng, X., et al., 2018. Visual evaluation method for fluids in cores based on low field nuclear magnetic resonance technology. Oilfield Chem. 35 (1), 170–175 (in Chinese).

Du, J., Liu, H., Ma, D., et al., 2014. Discussion on effective development techniques for continental tight oil in China. Petrol. Explor. Dev. 41 (2), 217–224. https://doi.org/10.1016/S1876-3804(14)60025-2.

Fu, Q., Cudjoe, S., Ghahfarokhi, R.B., et al., 2021. Investigating the role of diffusion in hydrocarbon gas huff-n-puff injection-an Eagle Ford study. J. Petrol. Sci. Eng. 198, 108146. https://doi.org/10.1016/j.petrol.2020.108146.

Gamadi, T.D., Sheng, J.J., Soliman, M.Y., et al., 2014. An experimental study of cyclic CO_2 injection to improve shale oil recovery. In: SPE Improved Oil Recovery Conference. https://doi.org/10.2118/169142-MS.

Gao, Y., Li, Q., He, X., et al., 2021. Quantitative evaluation of shale-oil recovery during CO_2 huff-n-puff at different pore scales. Energy Fuel. 35 (20), 16607–16616. https://doi.org/10.1021/acs.energyfuels.1c02734.

Hamdi, H., Clarkson, C.R., Ghanizadeh, A., et al., 2018. Huff-n-puff gas injection performance in shale reservoirs: a case study from Duvernay Shale in Alberta, Canada. In: SPE/AAPG/SEG Unconventional Resources Technology Conference. https://doi.org/10.15530/urtec-2018-2902835.

Hawthorne, S.B., Miller, D.J., Jin, L., et al., 2016. Rapid and simple capillary-rise/vanishing interfacial tension method to determine crude oil minimum miscibility pressure: pure and mixed CO_2, methane, and ethane. Energy Fuel. 30 (8), 6365–6372. https://doi.org/10.1021/acs.energyfuels. 6b01151.

Hoffman, B.T., 2018. Huff-n-puff gas injection pilot projects in the Eagle Ford. In: SPE Canada Unconventional Resources Conference. Society of Petroleum Engineers. https://doi.org/10.2118/189816-MS.

Huang, X., Ni, J., Li, X., et al., 2020. Characteristics and influencing factors of CO_2 flooding in different microscopic pore structures in tight reservoirs. Acta Pet. Sin. 41 (7), 853–864. https://doi.org/10.7623/syxb202007007 (in Chinese).

Huang, X., Dou, L., Zuo, X., et al., 2021. Dynamic imbibition and drainage laws of factures in tight reservoirs. Acta Pet. Sin. 42 (7), 924–935. https://doi.org/10.7623/syxb202107007 (in Chinese).

Huang, X., Li, X., Zhang, Y., et al., 2022. Microscopic production characteristics of crude oil in nano-pores of shale oil reservoirs during CO_2 huff and puff. Petrol. Explor. Dev. 49 (3), 636–643. https://doi.org/10.1016/S1876-3804(22)60053-3.

Kalra, S., Tian, W., Wu, X., 2018. A numerical simulation study of CO_2 injection for enhancing hydrocarbon recovery and sequestration in liquid-rich shales. Petrol. Sci. 15, 103–115. https://doi.org/10.1007/s12182-017-0199-5.

Li, C., Pu, H., Zhong, X., et al., 2020b. Interfacial interactions between Bakken crude oil and injected gases at reservoir temperature: a molecular dynamics simulation study. Fuel 276, 118058. https://doi.org/10.1016/j.fuel.2020.118058.

Li, L., Sheng, J.J., 2017. Numerical analysis of cyclic CH_4 injection in liquid-rich shale reservoirs based on the experiments using different-diameter shale cores and crude oil. J. Nat. Gas Sci. Eng. 39, 1–14. https://doi.org/10.1016/j.jngse.2017.01.017.

Li, L., Su, Y., Sheng, J.J., 2018. Investigation of gas penetration depth during gas huff-n-puff EOR process in unconventional oil reservoirs. In: SPE Canada Unconventional Resources Conference. https://doi.org/10.2118/189804-MS.

Li, S., Wang, Q., Zhang, K., Li, Z., 2020a. Monitoring of CO_2 and CO_2 oil-based foam flooding processes in fractured low-permeability cores using nuclear magnetic resonance (NMR). Fuel 263, 116648. https://doi.org/10.1016/j.fuel.2019.116648.

Li, Z., Qu, X., Liu, W., et al., 2015. Development modes of triassic yanchang formation chang 7 member tight oil in Ordos basin, NW China. Petrol. Explor. Dev. 42 (2), 241–246. https://doi.org/10.1016/S1876-3804(15)30011-2.

Luo, Y., Zheng, T., Xiao, H., et al., 2022. Identification of distinctions of immiscible CO_2 huff and puff performance in Chang-7 tight sandstone oil reservoir by applying NMR, microscope and reservoir simulation. J. Petrol. Sci. Eng. 209, 109719. https://doi.org/10.1016/j.petrol.2021.109719.

Ma, Q., Yang, S., Lv, D., et al., 2019. Experimental investigation on the influence factors and oil production distribution in different pore sizes during CO_2 huff-n-puff in an ultra-high-pressure tight oil reservoir. J. Petrol. Sci. Eng. 178, 1155–1163. https://doi.org/10.1016/j.petrol.2019.04.012.

Min, B., Mamoudou, S., Dang, S., et al., 2020. Comprehensive experimental study of huff-n-puff enhanced oil recovey in eagle ford: key parameters and recovery mechanism. In: SPE Improved Oil Recovery Conference. https://doi.org/10.2118/200436-MS.

Orozco, D., Fragoso, A., Selvan, K., et al., 2020. Eagle ford huff 'n' puff gas-injection pilot: comparison of reservoir-simulation, material balance, and real performance of the pilot well. SPE Reservoir Eval. Eng. 23 (1), 247–260. https://doi.org/10.2118/191575-PA.

Ozowe, W., Zheng, S., Sharma, M., 2020. Selection of hydrocarbon gas for huff-n-puff IOR in shale oil reservoirs. J. Petrol. Sci. Eng. 195, 107683. https://doi.org/10.1016/j.petrol.2020.107683.

Peng, Z., Sheng, J.J., 2023. Diffusion effect on shale oil recovery by CO_2 huff-n-puff. Energy Fuel. 37 (4), 2774–2790. https://doi.org/10.1021/acs.energyfuels.2c03871.

Sanchez-Rivera, D., Mohanty, K., Balhoff, M., 2015. Reservoir simulation and optimization of huff-and-puff operations in the Bakken shale. Fuel 147, 82–94. https://doi.org/10.1016/j.fuel.2014.12.062.

Shen, Z., Sheng, J.J., 2016. Experimental study of asphaltene aggregation during CO_2 and CH_4 injection in shale oil reservoirs. In: SPE Improved Oil Recovery Conference. https://doi.org/10.2118/179675-MS.

Sheng, J.J., 2017. Critical review of field EOR projects in shale and tight reservoirs. J. Petrol. Sci. Eng. 159, 654–665. https://doi.org/10.1016/j.petrol.2017.09.022.

Shilov, E., Dorhjie, D.B., Mukhina, E., et al., 2022. Experimental and numerical studies of rich gas huff-n-puff injection in tight formation. J. Petrol. Sci. Eng. 208, 109420. https://doi.org/10.1016/j.petrol.2021.109420.

Song, C., Yang, D., 2013. Performance evaluation of CO_2 huff-n-puff processes in tight oil formations. In: SPE Unconventional Resources Conference. https://doi.org/10.2118/167217-MS.

Song, C., Yang, D., 2017. Experimental and numerical evaluation of CO_2 huff-n-puff processes in Bakken formation. Fuel 190, 145–162. https://doi.org/10.1016/j.fuel.2016.11.041.

Song, Y., Song, Z., Zeng, H., Tai, C., Chang, X., 2022a. N_2 and CO_2 huff-n-puff for enhanced tight oil recovery: an experimental study using nuclear magnetic resonance. Energy Fuel. 36 (3), 1515–1521. https://doi.org/10.1021/acs.energyfuels.1c03982.

Song, Y., Song, Z., Zhang, Y., et al., 2022b. Pore scale performance evaluation and impact factors in nitrogen huff-n-puff EOR for tight oil. Petrol. Sci. 19 (6), 2932–2940. https://doi.org/10.1016/j.petsci.2022.05.012.

Sun, R., Yu, W., Xu, F., Pu, H., Miao, J., 2019. Compositional simulation of CO_2 Huff-n-Puff process in Middle Bakken tight oil reservoirs with hydraulic fractures. Fuel 236, 1446–1457. https://doi.org/10.1016/j.fuel.2018.09.113.

Syed, F.I., Muther, T., Van, V.P., Dahaghi, A.K., Negahban, S., 2022. Numerical trend analysis for factors affecting EOR performance and CO_2 storage in tight oil reservoirs. Fuel 316, 123370. https://doi.org/10.1016/j.fuel.2022.123370.

Tang, W., Sheng, J.J., Jiang, T., 2022. Further discussion of CO_2 huff-n-puff mechanisms in tight oil reservoirs based on NMR monitored fluids spatial distributions. Petrol. Sci. 20 (1), 350–361. https://doi.org/10.1016/j.petsci.2022.08.014.

Tran, S., Eghbali, S., Dehghanpour, H., 2020. Studying phase behavior of oil/natural-gas systems for designing gas-injection operations: a montney case study. SPE Reservoir Eval. Eng. 23 (3), 943–961. https://doi.org/10.2118/201109-PA.

Wang, H., Lun, Z., Lv, C., et al., 2018a. Nuclear-magnetic-resonance study on mechanisms of oil mobilization in tight sandstone reservoir exposed to carbon dioxide. SPE J. 23 (3), 750–761. https://doi.org/10.2118/179554-PA.

Wang, L., Tian, Y., Yu, X., et al., 2017. Advances in improved/enhanced oil recovery technologies for tight and shale reservoirs. Fuel 210, 425–445. https://doi.org/10.1016/j.fuel.2017.08.095.

Wang, M., Chen, S., Lin, M., 2018b. Enhancing recovery and sensitivity studies in an unconventional tight gas condensate reservoir. Petrol. Sci. 15, 305–318.

Wang, X., Xiao, P., Yang, Z., et al., 2020. Laboratory and field-scale parameter optimization of CO_2 huff–n–puff with the staged-fracturing horizontal well in tight oil reservoirs. J. Petrol. Sci. Eng. 186, 106703. https://doi.org/10.1016/j.petrol.2019.106703.

Wang, Y., Hu, J., Xie, W., et al., 2022. Optimization and analysis of CO_2 huff-n-puff process in shale oil reservoirs using response surface methodology (RSM). Geofluids, 5927853. https://doi.org/10.1155/2022/5927853, 2022.

Wei, B., Zhang, X., Wu, R., et al., 2019. Pore-scale monitoring of CO_2 and N_2 flooding processes in a tight formation under reservoir conditions using nuclear magnetic resonance (NMR): a case study. Fuel 246, 34–41. https://doi.org/10.1016/j.fuel.2019.02.103.

Xia, Y., Li, L., Wang, Z., 2022. Experimental and numerical study on influencing factors of replacement capacity and slickwater flowback efficiency using pre-CO_2 fracturing in tight oil reservoirs. J. Petrol. Sci. Eng. 215, 110697. https://doi.org/10.1016/j.petrol.2022.110697.

Yao, C., Liu, B., Liu, Y., et al., 2022. Quantitative investigation on natural gas flooding characteristics in tight oil cores after fracturing based on nuclear magnetic resonance technique. SPE J. 27 (6), 3757–3772. https://doi.org/10.2118/212835-PA.

Yang, P., Guo, H., Yang, D., 2013. Determination of residual oil distribution during waterflooding in tight oil formations with NMR relaxometry measurements. Energy Fuel. 27 (10), 5750–5756. https://doi.org/10.1021/ef400631h.

Yang, Y., Hu, Y., Zhu, Y., et al., 2023. Similarity-based laboratory study of CO_2 huff-n-puff in tight conglomerate cores. Petrol. Sci. 20 (1), 362–369. https://doi.org/10.1016/j.petsci.2022.09.030.

Yang, Z., Hou, L., Tao, S., et al., 2015. Formation conditions and "sweet spot " evaluation of tight oil and shale oil. Petrol. Explor. Dev. 42 (5), 555–565 (in Chinese).

Yu, H., Lu, X., Fu, W., Wang, Y., Xu, H., Xie, Q., Qu, X., Lu, J., 2020. Determination of

minimum near miscible pressure region during CO_2 and associated gas injection for tight oil reservoir in Ordos Basin, China. Fuel 263, 116737. https://doi.org/10.1016/j.fuel.2019.116737.

Yu, Y., Li, L., Sheng, J.J., 2017. A comparative experimental study of gas injection in shale plugs by flooding and huff-n-puff processes. J. Nat. Gas Sci. Eng. 38, 195–202. https://doi.org/10.1016/j.jngse.2016.12.040.

Zanganeh, P., Dashti, H., Ayatollahi, S., 2018. Comparing the effects of CH_4, CO_2, and N_2 injection on asphaltene precipitation and deposition at reservoir condition: a visual and modeling study. Fuel 217, 633–641. https://doi.org/10.1016/j.fuel.2018.01.005.

Zhang, X., Wei, B., You, J., et al., 2021. Characterizing pore-level oil mobilization processes in unconventional reservoirs assisted by state-of-the-art nuclear magnetic resonance technique. Energy 236, 121549. https://doi.org/10.1016/j.energy.2021.121549.

Zheng, T., Liu, X., Yang, Z., et al., 2021. Identification of seepage mechanisms for natural gas huff-n-puff and flooding processes in hydrophilic reservoirs with low and ultra-low permeabilities. J. Energy Resour. Technol. 143 (6), 063004. https://doi.org/10.1115/1.4048526.

Zuloaga, P., Yu, W., Miao, J., et al., 2017. Performance evaluation of CO_2 huff-n-puff and continuous CO_2 injection in tight oil reservoirs. Energy 134, 181–192. https://doi.org/10.1016/j.energy.2017.06.028.